

Electromagnetic nucleon form factors in the extended vector meson dominance model

K. S. Kuzmin,^{1,2,*} N. M. Levashko,^{2,†} and M. I. Krivoruchenko^{2,‡}

¹*Bogoliubov Laboratory of Theoretical Physics, Joint Institute for Nuclear Research,
RU-141980 Dubna, Russia*

²*National Research Centre “Kurchatov Institute”,
RU-123182 Moscow, Russia*

(Dated: January 22, 2025)

An extended vector meson dominance model is developed to describe electromagnetic nucleon form factors. The model includes families of the ρ - and ω -mesons with the associated radial excitations. The free parameters of the model are determined using a global statistical analysis of experimental data on the electromagnetic nucleon form factors in space- and timelike regions of transferred momenta. The vector meson masses and widths are equal to their empirical values, while the residues of form factors at the poles corresponding to the ground states of the ρ - and ω -mesons are consistent with the findings of both the Frazer-Fulco unitarity relations and the Bonn potential for coupling constants of the ρ - and ω -mesons with nucleons. Theoretical constraints imposed on the model include the quark counting rules, the Okubo-Zweig-Iizuka rule, the scaling law of Sachs form factors at moderate momentum transfers, and the suppression of Sachs form factors near the nucleon-antinucleon threshold. A reasonable description of the nucleon form factors in the experimentally accessible range of transferred momenta, as well as the electric and magnetic nucleon radii and Zemach radii, is obtained.

PACS numbers: 14.20.Dh, 25.75.Dw, 13.30.Ce, 12.40.Yx

I. INTRODUCTION

The investigation of the electromagnetic characteristics of nucleons remains an active topic in elementary particle physics. The electromagnetic form factors of nucleons provide information on the structure and interactions of nucleons with other fundamental particles. The form factors are analytical functions of the four-momentum transfer squared $t = q^2$. Their analytical properties are simple enough to allow the effective use of dispersion theories. Unitarity relations for electromagnetic pion and nucleon form factors [1–4], as well as quark counting rules (QCR’s) [5–8]

$$F_{1N}(t) = O(1/t^2), \quad (1.1)$$

$$F_{2N}(t) = O(1/t^3) \quad \text{as } t \rightarrow -\infty, \quad (1.2)$$

are important frameworks for gaining a deeper understanding of the form factor properties. The unitarity relations lead to the vector meson dominance (VMD) model. The final-state interaction theorem implies that the model admits an extension to include higher radial excitations of vector mesons. The extended vector meson dominance (eVMD) model can be merged with QCR’s. The eVMD model maintains gauge invariance of electromagnetic interactions [9] and thoroughly describes various kinds of processes [10–16].

In the 1960s, measurements of the nucleon form factors for the spacelike region with moderate momentum transfers $Q^2 = -q^2 \lesssim 1 \text{ GeV}^2$ revealed that Sachs form factors follow the scaling relations (SR’s)

$$G_{Ep}(t) = G_{Mp}(t)/\mu_p = G_{Mn}(t)/\mu_n, \quad (1.3)$$

where μ_N are the magnetic moments of nucleons in nuclear magnetons. The measured form factors can be parameterized using the dipole function

$$G_D(t) = \left(1 - \frac{t}{M_V^2}\right)^{-2}, \quad (1.4)$$

which corresponds to exponential radial charge and magnetization density distributions, where $M_V = 0.84 \text{ GeV}$ is the mass parameter of the vector channel. As momentum transfers expand, both SR’s and dipole dependence decrease in accuracy. The newest solutions involve advanced parameterizations [17–20], with the most accurate ones integrated into the Monte Carlo event generators to numerically simulate various types of processes for experiments.

The measurements of nucleon form factors for the timelike region of q^2 were a significant milestone in the study of nucleon form factors [21–29].

There are numerous theoretical schemes for describing the form factors of nucleons (see [30–32] for the review). Theoretical models are primarily phenomenological and have a variety of free parameters. The analyticity of form factors, QCR’s, and unitarity relations are essential for the development of models.

Up to isotopic factors, the vector component of the weak nucleon current corresponds to the photon vertex

* kkuzmin@theor.jinr.ru

† levashko_nm@mail.ru

‡ mikhail.krivoruchenko@itep.ru

allowing the weak process amplitudes to be constructed using data on the electromagnetic nucleon form factors. A thorough description of lepton interactions with nucleons is also required for processing and interpreting the results of experiments involving lepton scattering on nucleons, particularly for accelerator experiments (FNAL MiniBooNE, NO ν A, DUNE, projects at Kamiokande laboratory) to study the neutrino properties.

New measurements of nucleon form factors have been reported in recent years, with particular emphasis on the timelike region. The eVMD model [14] successfully reproduced earlier datasets with two free parameters. We will find that modifying only two parameters is insufficient to reproduce the data. The model parameters need to be updated to account for the larger dataset. In Sec. II, we describe the eVMD model in general and develop its

advanced version. Section III details the experimental data fitting methods and reports the new model parameter values, predictions for electric and magnetic nucleon radii, and vector meson-nucleon coupling constants. The model predictions for the form factors in comparison with the experimental data are shown in Figs. 1 – 9. The results are summarized in Conclusion.

II. EXTENDED VECTOR MESON DOMINANCE MODEL

Decomposition of the electromagnetic nucleon current by Lorentz covariant structures determines the electromagnetic form factors of nucleons, $F_{1N}(t)$ and $F_{2N}(t)$:

$$\langle p_f, s_f | J_{\text{em}}^\mu(q) | p_i, s_i \rangle = \bar{u}(p_f, s_f) \left(F_{1N}(t) \gamma^\mu + \frac{1}{2m_N} F_{2N}(t) i \sigma^{\mu\nu} q_\nu \right) u(p_i, s_i), \quad (2.1)$$

where $N = p$ for the proton and n for the neutron, m_N is the nucleon mass. The nucleon momenta in the final and initial states are represented by p_f and p_i , while the polarization vectors of the nucleons are represented by s_f and s_i . The momentum transfer is $q = p_f - p_i$, and $t = q^2$. The equation

$$F_{iI}(t) = \frac{1}{2} (F_{ip}(t) \pm F_{in}(t))$$

determines the isotopic components of the form factors; the upper and lower signs correspond to the isoscalar and isovector channels with $I = 0$ and 1, respectively. The matrices γ^μ and $\sigma^{\mu\nu}$ are defined as in [33].

Sachs form factors

$$G_{EN}(t) = F_{1N}(t) + \frac{t}{4m_N^2} F_{2N}(t), \quad (2.2)$$

$$G_{MN}(t) = F_{1N}(t) + F_{2N}(t) \quad (2.3)$$

are commonly used in analysing experimental data and their theoretical interpretation. The value $G_{MN}(0)$ is the nucleon magnetic moment in nuclear magnetons, while $F_{2N}(0)$ is its anomalous part. The value $F_{1N}(0)$ specifies the nucleon charge e_N in the proton charge units.

A. Constraints imposed on the eVMD models

1. Threshold identities

At the nucleon-antinucleon threshold ($N\bar{N}$), the electric (E) and magnetic (M) form factors satisfy the threshold identities (TI's):

$$G_{EN}(4m_N^2) = G_{MN}(4m_N^2). \quad (2.4)$$

The identities are a direct consequence of definitions (2.2) and (2.3), and they are obtained automatically when the parameterization is carried out using $F_{TN}(t)$. If form factors are parameterized in terms of $G_{TN}(t)$, then limitations (2.4) are applied as an extra requirement.

2. Quark counting rules

Hadron form factors obey QCR's [5–7]. Taking into account additional suppression of amplitudes, generated by spin flip of quarks [8], QCR's take the form of Eqs. (1.1) and (1.2) and give rise to

$$G_{EN}(t) \sim G_{MN}(t) = O(1/t^2) \quad \text{as } t \rightarrow -\infty. \quad (2.5)$$

The spin flip has a particularly substantial impact on the electromagnetic transitions of high-spin hadrons [8, 13, 15].

Electron-proton scattering experiments confirm QCR's up to $Q^2 \sim 10 \text{ GeV}^2$. The same holds true for the electromagnetic pion form factor. Quantum chromodynamics (QCD) predicts that the asymptotic regime for hadron form factors starts at $Q^2 \sim 100 \text{ GeV}^2$ (cf., e.g., the leading term and the next power term of the asymptotic decomposition of the pion form factor [34]). At intermediate momentum transfers, QCR's are still considered a phenomenological limitation.

3. Scaling relations

In the spacelike region for low momentum transfers Sachs form factors fulfill SR's (1.3). With acceptable accuracy $G_{Ep}(t)$, $G_{Mp}(t)/\mu_p$ and $G_{Mn}(t)/\mu_n$ are described

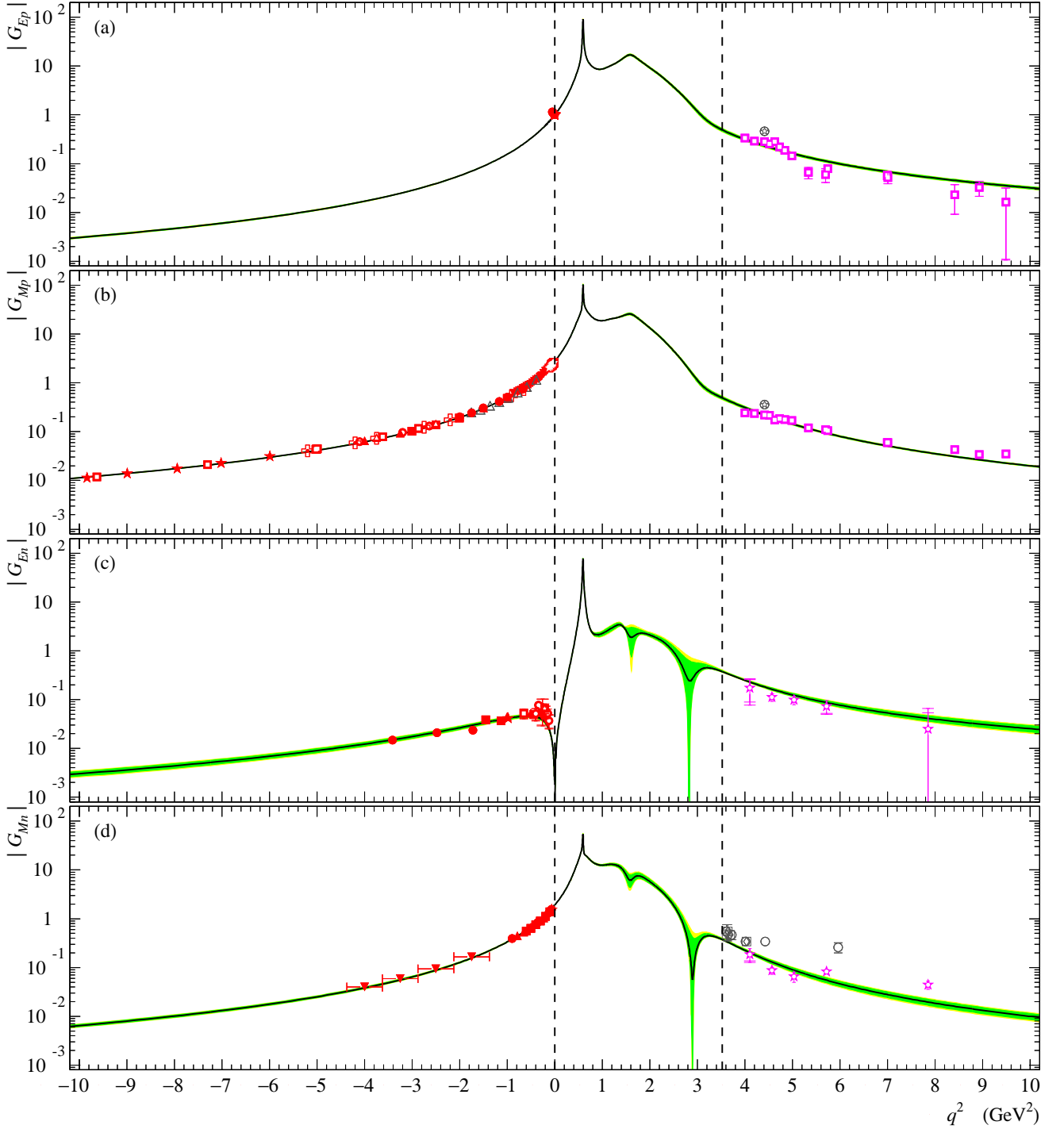


Figure 1. Modules of the electric and magnetic form factors of the proton (a, b) and neutron (c, d) for the space- and timelike regions of the four-momentum transfer squared predicted within the eVMD-VI model in comparison with the experimental data. Vertical dashed lines limit the experimentally unexplored region $0 < q^2 < 4m_N^2$.

by the dipole function (1.4). The asymptotic behavior of $G_D(t)$ is in agreement with QCR's.

Identity (2.4) does not contradict SR's, provided the Sachs form factors vanish at $t = 4m_N^2$. This assumption seemed to R. Feynman highly improbable [10], and it contradicts the present-day experiments: $|G_{Ep}(4m_N^2)| =$

0.401 ± 0.021 [35] and $|G_{En}(4m_N^2)| = 0.322 \pm 0.016$ [36] and 0.454 ± 0.062 [37]; the errors describe the statistical and systematic uncertainties.

It is noteworthy to mention, however, that the threshold values of nucleon form factors are small compared to

their values at zero momentum transfer:

$$|G_{Ep}(4m_N^2)| \sim \frac{1}{2} G_{Ep}(0) \sim \frac{1}{7} G_{Mp}(0), \quad (2.6)$$

$$|G_{En}(4m_N^2)| \sim \frac{1}{5} |G_{Mn}(0)|, \quad (2.7)$$

implying that SR's may still have an impact on the $N\bar{N}$ threshold.

In the spacelike region, when the momentum transfer increases up to $Q^2 \sim 3 \text{ GeV}^2$, the SR's violations become particularly obvious with regard to the ratio $G_{Ep}(t)/G_{Mp}(t)$ (see Sec. III).

Although SR's are performed approximately, they allow an accurate nonparametric description of an extensive array of experimental data at low momentum transfers.

4. Okubo-Zweig-Iizuka rule

According to the Okubo-Zweig-Iizuka (OZI) rule, mesons with valence strange quark-antiquark pairs are only weakly coupled to non-strange hadrons [38]. The theoretical explanation of this rule is based on the fact that annihilation of a strange quark-antiquark pair causes the appearance of a large momentum in the QCD coupling constant, resulting in amplitude suppression. The OZI rule suppresses contributions of strange vector mesons $\phi(1020)$ and their radial excitations to electromagnetic form factors of non-strange hadrons, including nucleons.

5. Analyticity

Analyticity is a universal attribute of quantum field theory, arising from causality and Lorentz covariance. Form factors are functions with the established analytical properties. The functions are analytical in the complex t -plane with a cut $(4m_\pi^2, +\infty)$ in the isovector channel and a cut $(9m_\pi^2, +\infty)$ in the isoscalar channel, where m_π is the pion mass. The class of analytical functions that meet these conditions is relatively vast, making it hard to severely constrain form factors based just on analyticity.

6. Frazer-Fulco unitarity

The formulation of two-body unitarity relations for the electromagnetic pion form factor [1, 4] and nucleon form factors [1–3] became a noteworthy achievement. The formalism used provides form factors with the correct analytical properties. The two-body unitarity is justified for spectral functions with the pion energy $t < 1 \text{ GeV}^2$. The pion form factor is expressed in terms of the mass and decay width of the ρ -meson. In the experimentally accessible energy range, it drops as $\sim 1/t$ in line with QCR's but asymptotically behaves like $1/\ln(-t)$ as $t \rightarrow -\infty$. In [34],

a model was proposed to correct the behavior of the pion form factor by taking into consideration the QCD asymptotics in the leading order together with preasymptotic power corrections. To evaluate spectral functions of nucleon form factors, experimental data on the pion-nucleon scattering amplitudes are required, and these amplitudes should be extrapolated into the non-physical region of positive t values [39, 40] (for a recent review, see [41]). The spectral functions exhibit a ρ -meson resonant contribution, validating the application of the VMD model in the isovector channel. According to quark models, the isoscalar ω -meson is the isotopic companion of the ρ -meson, so the isoscalar channel can be included in the VMD models.

B. eVMD₁ model

The VMD models violate the QCR's for nucleon form factors. Consequently, the model is modified by including radial excitations of ω - and ρ -mesons, the existence of which was first predicted in the Veneziano model [42]. The eVMD models that include isotopic families of vector mesons are widely used [11, 14–16, 43–46]. This subsection describes a class of eVMD models named the eVMD₁ that precisely match the requirements of TI's, QCR's, and SR's and are utilized as a first-order approximation in constructing realistic models of nucleon form factors.

In the no-width limit of vector mesons, the eVMD representation for Sachs form factors can be expressed as follows:

$$G_{TN}(t) = P_{n-2}^{TN}(t) \prod_V \frac{m_V^2}{m_V^2 - t}, \quad (2.8)$$

where $T = E, M$ indicates the type of form factors, $P_{n-2}^{TN}(t)$ is a polynomial of order $n-2$, n is the number of vector mesons, and $V = 1, \dots, n$. QCR's are satisfied identically owing to the multiplicative representation, whereas TI's impose the constraint $P_{n-2}^{EN}(4m_N^2) = P_{n-2}^{MN}(4m_N^2)$.

The multiplicative representation of the form factors is completely equivalent to the additive one:

$$G_{TN}(t) = P_{n-2}^{TN}(t) \sum_V \frac{1}{t - m_V^2} \text{res}_{u=m_V^2} \prod_{V'} \frac{m_{V'}^2}{m_{V'}^2 - u}.$$

The function (2.8) is rational, which ensures the decomposition into partial fractions. The residues of $F_{iI}(t)$ at $t = m_V^2$ determine the contributions of vector mesons to the form factors. The coupling constants f_{iI}^{VNN} of nucleons and vector mesons with isotopic spin I are identified as follows:

$$\frac{f_{iI}^{VNN}}{g_{\gamma V}} = -\frac{1}{m_V^2} \text{res}_{t=m_V^2} F_{iI}(t), \quad (2.9)$$

where $g_{\gamma V}$ stands for the vector meson coupling constants with photons.

The finite values of nucleon form factors at $t = 4m_N^2$ within the context of the considered model are attributed to corrections related to vector meson widths which lead to deviations from SR's. Incomplete degeneracy in masses of isoscalar and isovector mesons and a possible contribution of ϕ -mesons to nucleon form factors due to the approximate character of the OZI rule also violate SR's.

In the eVMD₁ model, the threshold values of the form factors are assumed to be zero. The polynomials $P_{n-2}^{TN}(t)$ are factorized to give

$$P_{n-2}^{TN}(t) = \left(1 - \frac{t}{4m_N^2}\right) P_{n-3}^{TN}(t).$$

The normalization conditions read $P_{n-3}^{EN}(0) = e_N$ and $P_{n-3}^{MN}(0) = \mu_N$. The polynomials of the magnetic form factors follow SR's and are expressed as

$$P_{n-3}^{Mp}(t)/\mu_p = P_{n-3}^{Mn}(t)/\mu_n = P_{n-3}^{Ep}(t).$$

The representations satisfy TI's, QCR's and SR's. There are $n-3$ parameters for each of the polynomials $P_{n-3}^{Ep}(t)$ and $P_{n-3}^{En}(t)$ to fit the experimental data.

The isotopic components of the form factors equal

$$F_{1I}(t) = \left(\left(e_I - \mu_I \frac{t}{4m_N^2} \right) P_{n-3}^{Ep}(t) \pm \frac{1}{2} P_{n-3}^{En}(t) \right) \prod_V \frac{m_V^2}{m_V^2 - t}, \quad (2.10)$$

$$F_{2I}(t) = \left((-e_I + \mu_I) P_{n-3}^{Ep}(t) \mp \frac{1}{2} P_{n-3}^{En}(t) \right) \prod_V \frac{m_V^2}{m_V^2 - t}, \quad (2.11)$$

where $e_I = (e_p \pm e_n)/2$ and $\mu_I = (\mu_p \pm \mu_n)/2$; the upper and lower signs indicate the isotopic scalars and vectors, respectively. The form factors $G_{TN}(t)$ include contributions of the isoscalar and isovector mesons. To eliminate contributions of isoscalar mesons from the isovector channel and vice versa, we could demand $P_{n-3}^{Ep}(m_V^2) = P_{n-3}^{En}(m_V^2) = 0$, which implies, however, that the meson V makes no contribution to the form factors. A non-trivial solution is conceivable for

$$\det \begin{vmatrix} e_I - \mu_I \frac{m_V^2}{4m_N^2} & \pm \frac{1}{2} \\ -e_I + \mu_I & \mp \frac{1}{2} \end{vmatrix} = 0.$$

This equation results in $m_V^2 = 4m_N^2$ and $G_{TN}(4m_N^2) \neq 0$, which contradicts SR's. To reconcile the representation with TI's, QCR's and SR's, the full ω/ρ degeneracy in masses of the ground and excited states of the ω - and ρ -mesons is required. In this case, the number of ω -mesons is equal to the number of ρ -mesons. To keep poles simple in the multiplicative representation, the parameter n should be regarded as the number of mesons in the family of either isoscalar or isovector mesons.

Equations (2.10) and (2.11) with two polynomials $P_{n-3}^{Ep}(t)$ and $P_{n-3}^{En}(t)$ define the eVMD₁ model that strictly meets the requirements of TI's, QCR's and SR's. The fundamental aspects are as follows: the presence of n vector mesons in isoscalar and isovector channels, the mass degeneracy of isoscalar and isovector mesons, and the meson zero widths. Strange vector mesons do not find a place in the eVMD₁ model since each channel has the same number of vector mesons, which is in line with the OZI rule.

The approximate nature of the OZI rule limits the precision of SR's to $O(f_{i0}^{\phi NN}/f_{i0}^{\omega NN})$. Of course, realistic models account for the widths of vector mesons. In the model discussed in the next section, vector meson widths vanish below the two- or three-pion threshold. The meson widths, as a result, produce no effect on spatial behavior of the form factors. When the form factors are analytic functions of t , the widths of vector mesons typically modify spacelike asymptotes via the dispersion integrals. Restoring QCR's requires imposing conditions of convergence and superconvergence of the dispersion integrals on the model parameters.

In the most basic scenario of $n = 3$, the key eVMD₁ model parameters are determined without directly addressing the experimental data. The normalization condition $P_{n-3}^{EN}(0) = e_N$ becomes the identity $P_{n-3}^{EN}(t) = e_N$, which results in

$$F_{1N}(t) = \left(e_N - \mu_N \frac{t}{4m_N^2} \right) \prod_V \frac{m_V^2}{m_V^2 - t}, \quad (2.12)$$

$$F_{2N}(t) = (-e_N + \mu_N) \prod_V \frac{m_V^2}{m_V^2 - t}. \quad (2.13)$$

C. eVMD models

The MFK model [14] with three meson states in each isotopic channel incorporates two free parameters c_N to account for deviations from SR's. It gives the numerator of $F_{1N}(t)$ a less specific structure: $e_N - c_N t$. Equation (2.12) suggests $c_N = -\mu_N/(4m_N^2)$. The parameter values of the $n = 3$ eVMD₁ model for $c_p = -0.79 \text{ GeV}^{-2}$

and $c_n = 0.54 \text{ GeV}^{-2}$ are qualitatively comparable to the values $c_p = -0.46 \text{ GeV}^{-2}$ and $c_n = 0.30 \text{ GeV}^{-2}$ extracted in [14] from the data. Table 1 compares the predicted coupling constants of the ω - and ρ -mesons with nucleons to those of other models. It also displays the electric and magnetic nucleon radii given by Eqs. (2.23) and (2.24) for $h_N = 0$.

In recent years, an extensive array of new experimental data on nucleon form factors was accumulated, while obvious deviations from the predictions of the MFK model emerged in the timelike region. The model has two free parameters only because of the implementation of the basic assumptions of the eVMD model for $n = 3$, while parameterizations and phenomenological models of nucleon form factors typically contain more than a dozen free parameters [16–20, 45, 47]. Our calculations indicate that adding the latest experimental data and simply redefining the parameters c_p and c_n is not enough to reach satisfactory agreement. A more thorough generalization of the MFK model should be provided. The current generalization addresses the following aspects:

i) To cope with the problem of timelike momenta, we introduce ω - and ρ -mesons with masses of 1.70 GeV , which are closest to the $N\bar{N}$ threshold. The timelike behavior of the form factors is expected to be sensitive to these mesons, although their influence on the space-like region is less obvious. Adding one pair of vector

mesons increases the number of free parameters in the model from two to six.

To describe small variations of nucleon form factors near the threshold, two more hypothetical mesons in each of the isotopic channels were introduced in [16]. These mesons are almost twice as heavy as nucleons and have widths of about 1 GeV .

ii) The second adjustment concerns the parameterization of vector meson widths. To guarantee that the form factors are continuous functions, the widths become dependent on the four-momentum transfer squared. The parameterization [48] of isoscalar vector meson widths, $\Gamma_V(t)$, at $t < t_0 < m_V^2$ employs the Gell-Mann, Sharp and Wagner formula [49]. In the isovector channel, the width is proportional to the two-pion phase space volume multiplied by the pion four-momentum squared in the center-of-mass frame. At $t > m_V^2$, the widths are regarded constant. The value of t_0 in both the cases is defined by the condition of matching continuously the function and its first derivative at $t = t_0$ and $t = m_V^2$ with the interpolating second-degree polynomial at $t_0 < t < m_V^2$. Below the three-pion threshold, the isoscalar vector mesons have zero widths. The isovector mesons have zero widths below the two-pion threshold. At $t = m_V^2$, the meson widths are adjusted to the experimental values.

In the modified model, the most general expression for the form factors takes the form

$$F_{1I}(t) = \sum_V P_{n-2}^{1I}(m_V^2) \frac{1}{t - m_V^2 + i\sqrt{t}\Gamma_V(t)} \text{res}_{u=m_V^2} \prod_{V'} \frac{m_{V'}^2}{m_{V'}^2 - u},$$

$$F_{2I}(t) = \sum_V P_{n-3}^{2I}(m_V^2) \frac{1}{t - m_V^2 + i\sqrt{t}\Gamma_V(t)} \text{res}_{u=m_V^2} \prod_{V'} \frac{m_{V'}^2}{m_{V'}^2 - u},$$

where $P_k^{iI}(t)$ are polynomials of order k that can be expressed in terms of $P_{n-2}^{TN}(t)$ with the use of Eqs. (2.2) and (2.3). The pole at $t = 4m_N^2$, which emerges when inverting Eqs. (2.2) and (2.3), is fictitious due to the TIs. The summation runs over the ground and excited states of vector mesons with isospin I .

The polynomials for the four vector meson states have the parameterization

$$P_2^{1I}(t) = e_I + c_I t + d_I t^2, \quad (2.14)$$

$$P_1^{2I}(t) = -e_I + \mu_I + h_I t, \quad (2.15)$$

where $c_I = (c_p \pm c_n)/2$ for isotopic scalars (+) and vectors (−), respectively, and the similarly for d_I and h_I . This model is referred to as the eVMD-VI model, where the number VI denotes the number of fitted model parameters.

D. Moments of nucleon radii

Electric and magnetic moments of nucleon radii are determined by charge and magnetization density distributions in the Breit frame of nucleons:

$$\langle r^s \rangle_{TN} = \int d\mathbf{r} r^s \rho_{TN}(\mathbf{r}). \quad (2.16)$$

The identification of $\rho_{TN}(\mathbf{r})$ with the Fourier transforms of the electric form factors $\mathcal{G}_{EN}(t) \equiv G_{EN}(t)$ and the normalized magnetic form factors $\mathcal{G}_{MN}(t) \equiv G_{MN}(t)/G_{MN}(0)$,

$$\rho_{TN}(\mathbf{r}) = \int \frac{d\mathbf{Q}}{(2\pi)^3} e^{i\mathbf{Q}\mathbf{r}} \mathcal{G}_{TN}(-\mathbf{Q}^2), \quad (2.17)$$

leads to the equations

$$\langle r^{2s+1} \rangle_{TN} = \frac{(2s+2)!}{\pi} \int_{-\infty}^0 \frac{\mathcal{G}_{TN}^{\text{reg}}(t)}{t^{s+1}\sqrt{-t}} dt, \quad (2.18)$$

$$\langle r^{2s} \rangle_{TN} = \frac{(2s+1)!}{s!} \left. \frac{d^s \mathcal{G}_{TN}(t)}{dt^s} \right|_{t=0}, \quad (2.19)$$

where $s = 1, 2, \dots$ and

$$\mathcal{G}_{TN}^{\text{reg}}(t) = \mathcal{G}_{TN}(t) - \sum_{k=0}^s \frac{t^k}{k!} \left. \frac{d^k \mathcal{G}_{TN}(t)}{dt^k} \right|_{t=0}.$$

The expansion at $t = 0$ goes over the integer powers of t because the form factors are analytical functions in a neighborhood of $t = 0$. The derivation of Eqs. (2.18) and (2.19) is given in Appendix A.

In the region $\Re(t) < 0$ of the complex t -plane, the form factors are analytical functions, too. The analytical continuation of the form factors in the region $\Re(t) \geq 0$ leads to the eVMD model with zero widths of vector mesons. The only singularities of the form factors are the thresholds and simple poles corresponding to the vector meson masses. The integration in Eq. (2.18) is assumed to run along the upper edge of the cut $(-\infty, 0)$. Bypassing the square root singularity at $t = 0$, we complement it with an integral in the opposite direction along the lower edge of the cut. We close the contour at infinity and, using Cauchy's theorem, obtain in the model under consideration

$$\langle r^{2s+1} \rangle_{TN} = (2s+2)! \sum_V \frac{\tilde{f}_{TN}^{VNN}}{g_{\gamma V}} \frac{1}{m_V^{2s+1}}, \quad (2.20)$$

$$\langle r^{2s} \rangle_{TN} = (2s+1)! \sum_V \frac{\tilde{f}_{TN}^{VNN}}{g_{\gamma V}} \frac{1}{m_V^{2s}}, \quad (2.21)$$

where (cf. (2.9))

$$\frac{\tilde{f}_{TN}^{VNN}}{g_{\gamma V}} = -\frac{1}{m_V^2} \text{res}_{t=m_V^2} \mathcal{G}_{TN}(t). \quad (2.22)$$

The important case of the second moments allows the result to be presented in terms of the model parameters in a simple way:

$$\frac{1}{6} \langle r^2 \rangle_{EN} = c_N + \frac{\mu_N - e_N}{4m_N^2} + e_N \sum_V \frac{1}{m_V^2}, \quad (2.23)$$

$$\frac{1}{6} \langle r^2 \rangle_{MN} = \frac{c_N + h_N}{\mu_N} + \sum_V \frac{1}{m_V^2}. \quad (2.24)$$

Zemach moments of the charge and magnetization distributions of the proton arise in the theory of Lamb shift and hyperfine interactions. They are defined by convolution of the charge distribution density with the charge or magnetization distribution density of the proton:

$$\langle r^s \rangle_{ET} = \int d\mathbf{r} r^s \varrho_{ET}(\mathbf{r}),$$

where

$$\varrho_{ET}(\mathbf{r}) = \int d\mathbf{r}' \rho_{Ep}(\mathbf{r} - \mathbf{r}') \rho_{Tp}(\mathbf{r}').$$

In terms of proton form factors, using the Fourier transform, the moments take the form:

$$\langle r^{2s+1} \rangle_{ET} = \frac{(2s+2)!}{\pi} \int_{-\infty}^0 \frac{(G_{Ep}(t) \mathcal{G}_{Tp}(t))^{\text{reg}}}{t^{s+1} \sqrt{-t}} dt, \quad (2.25)$$

$$\langle r^{2s} \rangle_{ET} = \sum_{k=0}^s \frac{(2s+1)! \langle r^{2k} \rangle_{Ep} \langle r^{2s-2k} \rangle_{Tp}}{(2s-2k+1)! (2k+1)!}, \quad (2.26)$$

where

$$(G_{EN}(t) \mathcal{G}_{TN}(t))^{\text{reg}} = G_{EN}(t) \mathcal{G}_{TN}(t) - \sum_{k=0}^s \frac{t^k}{k!} \left. \frac{d^k G_{EN}(t) \mathcal{G}_{TN}(t)}{dt^k} \right|_{t=0}.$$

In the eVMD models under consideration,

$$\begin{aligned} \langle r^{2s+1} \rangle_{ET} = & (2s+2)! \sum_{V \neq V'} \frac{\tilde{f}_{Ep}^{VNN} \tilde{f}_{Tp}^{V'NN}}{g_{\gamma V} g_{\gamma V'}} \times \\ & \frac{m_V^{2s+3} - m_{V'}^{2s+3}}{m_V^{2s+1} m_{V'}^{2s+1} (m_V^2 - m_{V'}^2)} \\ & + \frac{(2s+3)!}{2} \sum_V \frac{\tilde{f}_{Ep}^{VNN} \tilde{f}_{Tp}^{VNN}}{g_{\gamma V} g_{\gamma V} m_V^{2s+1}}, \end{aligned}$$

while the even moments $\langle r^{2s} \rangle_{ET}$ are determined by Eqs. (2.21) and (2.26).

III. GLOBAL FIT PROCEDURE AND RESULTS

The model parameters c_I , d_I , and h_I are determined by fitting the experimental data. Masses and widths and other physical inputs are taken according to the most recent data, as suggested by PDG [50]. The evidence for a 1.25 GeV resonances is reported in [51–54]. The following set of vector meson masses (given in GeV) is used: $m_\rho = m_\omega = 0.77$, $m_{\rho'} = m_{\omega'} = 1.25$, $m_{\rho''} = m_{\omega''} = 1.45$, and $m_{\rho'''} = m_{\omega'''} = 1.70$. The widths of vector meson states (given in GeV) are $\Gamma_\rho = 0.15$, $\Gamma_\omega = 0.0085$, $\Gamma_{\rho'} = 0.3$, $\Gamma_{\omega'} = 0.13$, $\Gamma_{\rho''} = 0.4$, $\Gamma_{\omega''} = 0.29$, $\Gamma_{\rho'''} = 0.25$, and $\Gamma_{\omega'''} = 0.315$.

A. Data collection

The proton and neutron electromagnetic form factors were measured for space- and timelike regions of q^2 with the Thomas Jefferson National Accelerator Facility (JLab) [55–75], National Accelerator Laboratory Stanford Linear Accelerator Center (SLAC) [76–85], Massachusetts Institute of Technology Bates Linear Accelerator Center (MIT BLAC) [86–89], Cornell Electron Storage Ring (CESR) [90], Brookhaven National Laboratory (BNL) [25], Nationaal Instituut voor Kernfysica en Hoge Energie-Fysica (NIKHEF) [91–93], Deutsches Elektronen-Synchrotron (DESY) [94], Bonn University

Electron Synchrotron (BUES) [95], Institute for Nuclear Physics of the University of Mainz, Mainz Microtron (MAMI) [96–103], Mainz Electron Linear Accelerator (MELA) [104, 105], Laboratoire de l’Accélérateur Linéaire Université de Paris-Sud Orsay Colliding Beam Facility (ODCI) [26, 27, 106–108], Adone e^+e^- Storage Ring in Frascati (FSR) [21, 22, 28, 29, 109, 110], European Organization for Nuclear Research (CERN) [23, 24, 111, 112], Budker INP VEPP-2000 e^+e^- Collider (BINP) [36, 37, 113–117], and Beijing Spectrometer at the Electron Positron double-ring collider (BES) [35, 118–123].

The data of G_{Ep}/G_D [103, 105] (40 data points), $G_{Mp}/(\mu_p G_D)$ [55, 56, 74, 76–79, 81, 94, 96, 104, 124] (84), $\mu_p G_{Ep}/G_{Mp}$ [58–60, 64, 68–71, 73, 87, 88] (57), G_{En} [57, 62, 65, 72, 86, 89, 92, 93, 98, 99] (22) $G_{Mn}/(\mu_n G_D)$ [63, 80, 91, 97, 101] (19), $\mu_n G_{En}/G_{Mn}$ [62, 65, 89, 102] (11), $|G_p|$ [23, 85, 111, 112, 114, 121] (73) $|G_{Ep}|$ [121] (16), $|G_{Mp}|$ [121] (16), $|G_{Ep}/G_{Mp}|$ [85, 114, 121] (23), $|G_n|$ [36, 113, 116] (19), $|G_{En}|$ [123] (5), $|G_{Mn}|$ [123] (5), and $|G_{En}/G_{Mn}|$ [123] (5) were selected for statistical analysis. The total set of 395 points consists of 233 and 162 points for the space- and time-like region, respectively. The proton form factors are studied significantly better than the neutron form factors. The global fit data set consists of 78% and 22% of the proton and neutron data points, respectively.

The data measured with SLAC 1966 [76], 1970 [77], 1989 [78], 1993 [79], DESY 1973 [94] and BUES 1971 [95], SLAC 1994 [81] were revisited by Brash *et al.* [124] and Arrington [125], respectively.

To distinguish the values of $|G_{EN}(t)|$ and $|G_{MN}(t)|$ above the $N\bar{N}$ threshold, the angular distribution of the final particles is measured. Most of the existing data are given for the effective form factor

$$G_N^{\text{eff}}(t) = \sqrt{\frac{|G_{EN}(t)|^2 + \eta |G_{MN}(t)|^2}{1 + \eta}}, \quad (3.1)$$

where $\eta = t/(2m_N^2)$, extracted from the total cross sections. The current analysis uses the data that are not based on the assumption $|G_{EN}(t)| = |G_{MN}(t)|$.

Data analyses mainly use the single-photon exchange approximation, which is justified for low momentum transfers. The corrections associated with the two-photon exchange approach (0.2–0.6)% at $Q^2 \sim 4 \text{ GeV}^2$ for the proton and increase with Q^2 , causing some uncertainty in the measurement data. Data analysis including a theoretical description of two-photon exchange and radiative corrections provides an improved evaluation of the form factor values and measurement errors [47].

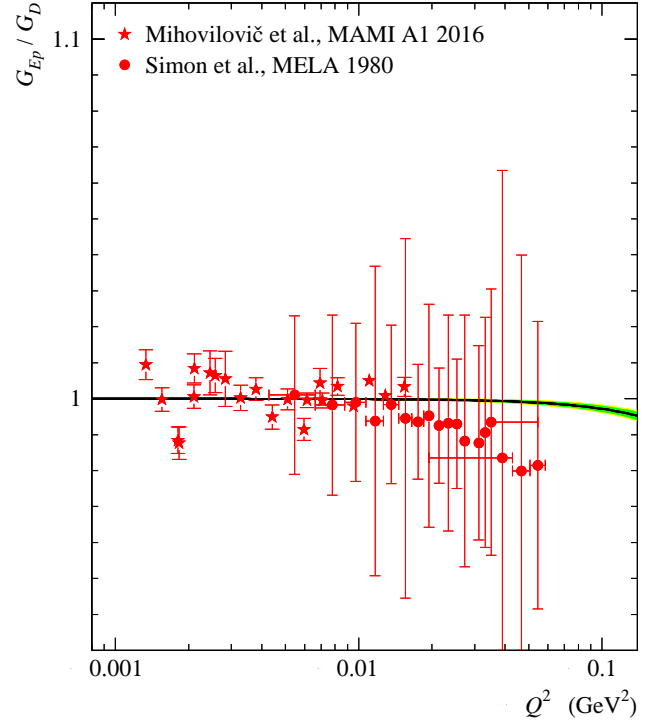


Figure 2. Normalized electric form factor of the proton measured for the spacelike region with MAMI A1 2016 [103] and MELA 1980 [105] in comparison with the eVMD-VI model.

B. Data analysis

We use the simplest form of the chi-squared function

$$\chi^2(\theta) = \sum_{t_s < 0} \left(\frac{\mathcal{F}(t_s, \theta) - \mathcal{F}_s^{\text{exp}}}{\Delta \mathcal{F}_s^{\text{exp}}} \right)^2 + \sum_{t_s > 0} \left(\frac{|\mathcal{F}(t_s, \theta)| - |\mathcal{F}_s^{\text{exp}}|}{\Delta |\mathcal{F}_s^{\text{exp}}|} \right)^2, \quad (3.2)$$

where $\mathcal{F}(t, \theta)$ is one of the form factors $F_{iN}(t)$, $G_{TN}(t)$, or $G_N^{\text{eff}}(t)$, and $\mathcal{F}_s^{\text{exp}}$ is its experimental value for $t = t_s$ with experimental error $\Delta \mathcal{F}_s^{\text{exp}}$. The data points are enumerated by the index s , and the parameter set is $\theta = (c_p, d_p, h_p, c_n, d_n, h_n)$. The theoretical values of $\mathcal{F}(t_s, \theta)$ are averaged over the experimental errors of the four-momentum transfer squared, as provided in the original papers. When uncertainties are not supplied, the error is assumed to be the difference between neighboring t_s values. In Eq. (3.2), the first term includes data from the spacelike region, while the second term includes data for the timelike region based on the measured absolute form factor values.

When the upper and lower errors in form factors differ, the chi-squared estimation uses their root mean square values. The errors used in Eq. (3.2) are calculated from statistical and systematic errors. The chi-squared function incorporates all data points with equal weights and no further constraints about possible normalization to

Table 1. The parameters c_p , d_p , h_p , c_n , d_n , and h_n of the eVMD₁, MFK, and the eVMD-VI models. The parameter values supplied with 1σ (2σ) errors correspond to the eVMD-VI model. The values of the coupling constants of vector mesons with nucleons are given in comparison with the estimates based on the unitarity relations for isovector nucleon form factors [126–128] and predictions of the boson exchange NN interaction Bonn model [129]. The values of electric and magnetic nucleon radii squared are also provided (see explanations in the text).

Parameters, couplings, radii	eVMD ₁ model	MFK model [14]	eVMD-VI model	PDG 2024 [50]	Ref. [126]	Ref. [127]	Ref. [128]	Bonn model [129]
c_p [GeV ⁻²]	-0.792	-0.463	-0.812±0.008(0.011)					
d_p [GeV ⁻⁴]	—	—	0.221±0.003(0.004)					
h_p [GeV ⁻²]	—	—	-0.552±0.009(0.011)					
c_n [GeV ⁻²]	0.542	0.297	0.256±0.016(0.022)					
d_n [GeV ⁻⁴]	—	—	-0.110±0.010(0.013)					
h_n [GeV ⁻²]	—	—	0.650±0.039(0.052)					
$f_{10}^{\omega NN}$	16.4	17.2	17.1					15.9
$f_{20}^{\omega NN}$	-2.31	-2.47	-1.50					0
$f_{11}^{\rho NN}$	1.18	3.02	3.43		5.8	2.61±0.40	-0.15±1.81	3.2
$f_{21}^{\rho NN}$	20.9	20.8	21.3		15.5	15.8±2.87	14.0±0.60	19.8
$\langle r^2 \rangle_{Ep}^{1/2}$ [fm]	0.77	0.82	0.815	0.8409±0.0004				
$\langle r^2 \rangle_{En}$ [fm ²]	0	-0.06	-0.067	-0.1155±0.0017				
$\langle r^2 \rangle_{Mp}^{1/2}$ [fm]	0.77	0.78	0.788	0.851±0.026				
$\langle r^2 \rangle_{Mn}^{1/2}$ [fm]	0.77	0.79	0.791	0.864 ^{+0.009} _{-0.008}				

specific form factor values are applied. The chi-squared minimization is performed using the CERN function minimization and error analysis package MINUIT (version 94.1) [130, 131]. The errors of the parameters quoted below correspond to the one- and two-standard deviation (1σ and 2σ) errors.

To assess the uncertainties in the model parameters, we first simulate a number of virtual experiments, the measurement results of which are determined by a normal distribution of the form factor values relative to the average and error of the form factors of the real experiment. The chi-square function is minimized to determine the model parameters for each simulation. At the final stage of the “bootstrap”, based on the sample of 10^4 virtual experiments, the average value and 1σ (2σ) variance of the parameters θ are found to be (given in GeV⁻²)

$$\begin{aligned}
 c_p &= -0.812 \pm 0.009(0.012), & c_n &= 0.256 \pm 0.018(0.025), \\
 d_p &= 0.221 \pm 0.003(0.004), & d_n &= -0.110 \pm 0.011(0.015), \\
 h_p &= -0.552 \pm 0.010(0.013), & h_n &= 0.650 \pm 0.044(0.058).
 \end{aligned}$$

The uncertainties in the parameters θ can alternatively be determined by directly generating an error ellipsoid from the error covariance matrix and, separately, using the standard package integrated into MINUIT. We use a flat prior probability density function of the parameters for evaluation of the posterior probability density function within the Bayesian method. The ellipsoids of errors in the parameter space are determined from the

equation $\chi^2(\theta) = \chi^2(\theta^*) + \text{constant}$, where θ^* denotes the parameter set values found by minimizing the chi-squared function [132]. Our calculations based on the error covariance matrix data are entirely consistent with the MINUIT algorithm. The parameter values together with their 1σ and 2σ errors are shown in Tab. 1. Our estimates also agree with the “bootstrap” method.

The minimal value of $\chi^2/\text{ndf} = 4443.3/(395-6) \approx 11.4$ for the current model corresponds to the parameter values supplied with 1σ (2σ) errors. The eVMD-VI model reproduces the observational data for the space- and timelike regions with about equal precision, although the number of points for the timelike region is two times less. The χ^2/ndf values calculated for the space- and timelike data sets with the values of the eVMD-VI model obtained from the global fit are $1948.5/227 \approx 8.6$ and $1543.3/156 \approx 9.9$, respectively. The χ^2/ndf values from separate fits of the space- and timelike data are $2794.4/227 \approx 12.3$ and $809.8/156 \approx 5.2$, respectively. Analysis shows that it is not possible to describe the data of the spacelike region using the model tuned to timelike data and vice versa. The parameters of the model and pairwise two-dimensional projections of error ellipsoids obtained from separate analyses of proton or neutron form factor data in the space-time domain only, or in both regions, are inconsistent with the corresponding values obtained from the global analysis. These findings point to the settings of the model parameters in a global

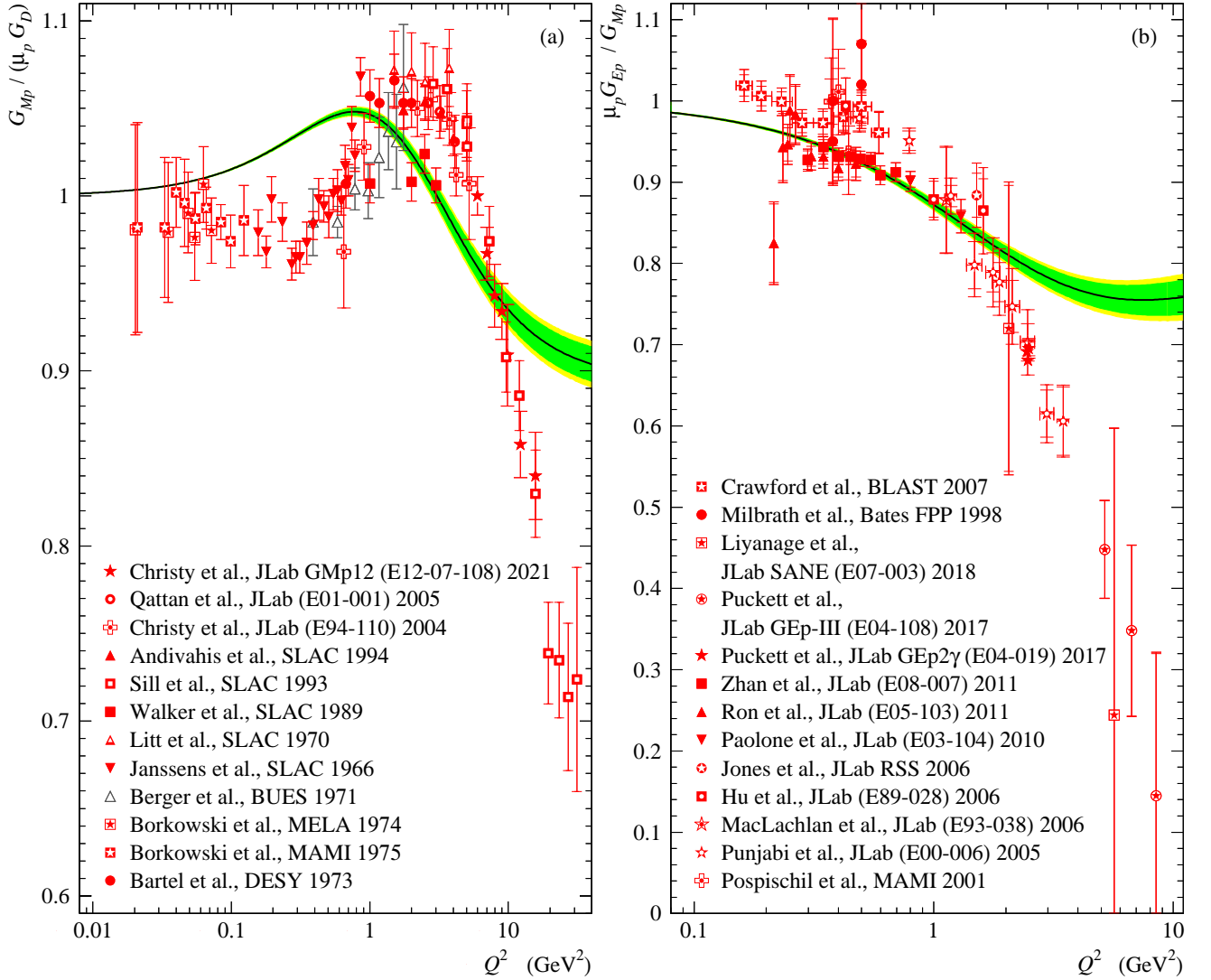


Figure 3. Normalized magnetic form factor of the proton (a) and the ratio of normalized electric to magnetic form factors of the proton (b) measured for the spacelike region with BLAST 2007 [88], MIT Bates FPP 1998 [87], JLab Hall A GMp12 (E12-07-108) 2021 [74], Hall C SANE (E07-003) 2018 [73], GEp-III (E04-108) 2017 [71], GEp2γ (E04-019) 2017 [67, 71], (E03-104) 2010 [68], Hall A (E05-103) 2011 [70], (E08-007) 2011 [69], Hall C RSS 2006 [60], Hall A (E89-028) 2006 [59], (E93-038) 2006 [64], (E01-001) 2005 [56], (E00-006) 2005 [58], (E94-110) 2004 [55], SLAC 1994 [81], 1993 [79], 1989 [78], 1970 [77], 1966 [76], BUES 1971 [95], MELA 1974 [104], MAMI 2001 [100], 1975 [96], and DESY 1973 [94] in comparison with the eVMD-VI model.

analysis of all data for both q^2 regions.

C. Numerical results for moments of nucleon radii

The numerical values of the second moments obtained in the model are displayed in Tab. 1 together with the experimental values. The coupling constants f_i^{VNN} are calculated based on Eq. (2.9) with the vector meson-photon coupling constants $g_{\omega\gamma} = 17.1$ and $g_{\rho\gamma} = 5.03$ [12] determined from the $\omega, \rho \rightarrow e^+e^-$ decays. The coupling constant errors of [40] are evaluated from the claimed accuracy $\pm 15\%$ of the πN scattering amplitudes.

The Zemach moments are required for calculating hy-

perfine splitting and the Lamb shift in hydrogen and muonic atoms. The numerical values of the moments are $\langle r \rangle_{EE} = 1.034$ fm and $\langle r \rangle_{EM} = 1.015$ fm are found to be close to the empirical values $\langle r \rangle_{EE}^{\text{exp}} = 1.085 \pm 0.003$ fm and $\langle r \rangle_{EM}^{\text{exp}} = 1.045 \pm 0.004$ fm [133] obtained from the analysis of the electron-proton scattering data [134, 135]. The value of the third Zemach moment equals $\langle r^3 \rangle_{EM} = 2.036$ fm³. The experimental values derived from the electron-proton scattering data are $\langle r^3 \rangle_{EM}^{\text{exp}} = 2.71 \pm 0.13$ fm³ [136] and 2.85 ± 0.08 fm³ (see [133] and references therein). The recent global analysis of the nucleon form factors gives $\langle r \rangle_{EE}^{\text{exp}} = 1.054^{+0.003+0.000}_{-0.014-0.015}$ fm and $\langle r^3 \rangle_{EM}^{\text{exp}} = 2.310^{+0.022+0.018}_{-0.014-0.015}$ fm³ [16], where the first and second errors are statistical and systematic, respectively.

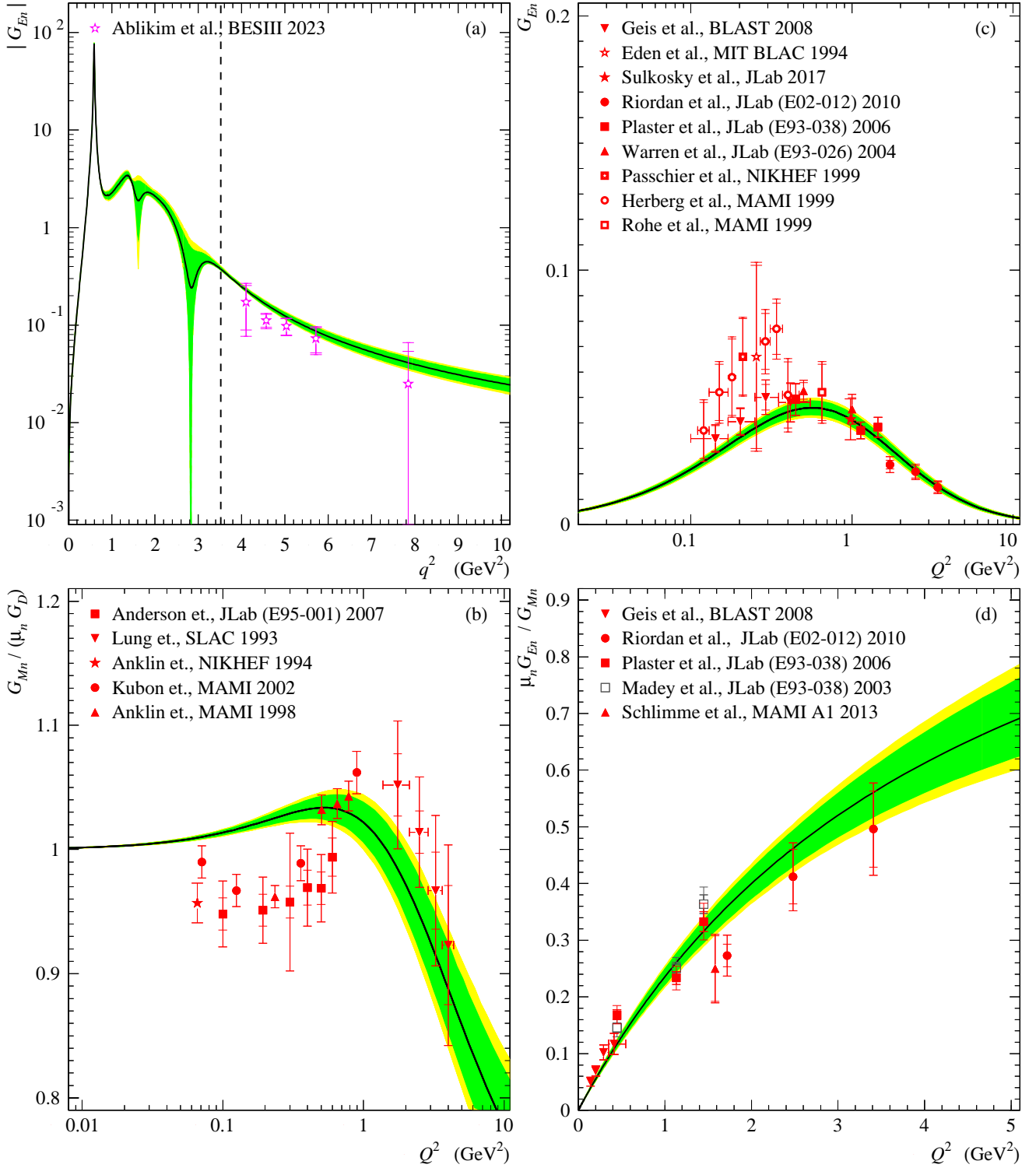


Figure 4. Module of electric form factor of the neutron (a) measured for the timelike region with BESIII 2023 [123]; normalized magnetic form factor of the neutron (b), electric form factor of the neutron (c), and the ratio of normalized electric to magnetic form factors of the neutron (d) measured for the spacelike region with BLAST 2008 [89], MIT BLAC 1994 [86], JLab Hall A 2017 [72], (E02-012) 2010 [65], (E95-001) 2007 [63], Hall C (E93-038) 2006 [62] (previous rapidly published result [61] is also shown), (E93-026) 2004 [57], NIKHEF 1999 [92] MAMI 1999 [98, 99], SLAC 1993[80], NIKHEF 1994 [91], MAMI A1 2013 [102], MAMI 2002 [101], and 1998 [97] in comparison with the eVMD-VI model. The data from [61, 102] are normalized on μ_n .

Except for the neutron charge radius, which is small, the moments of nucleon radii in the model under con-

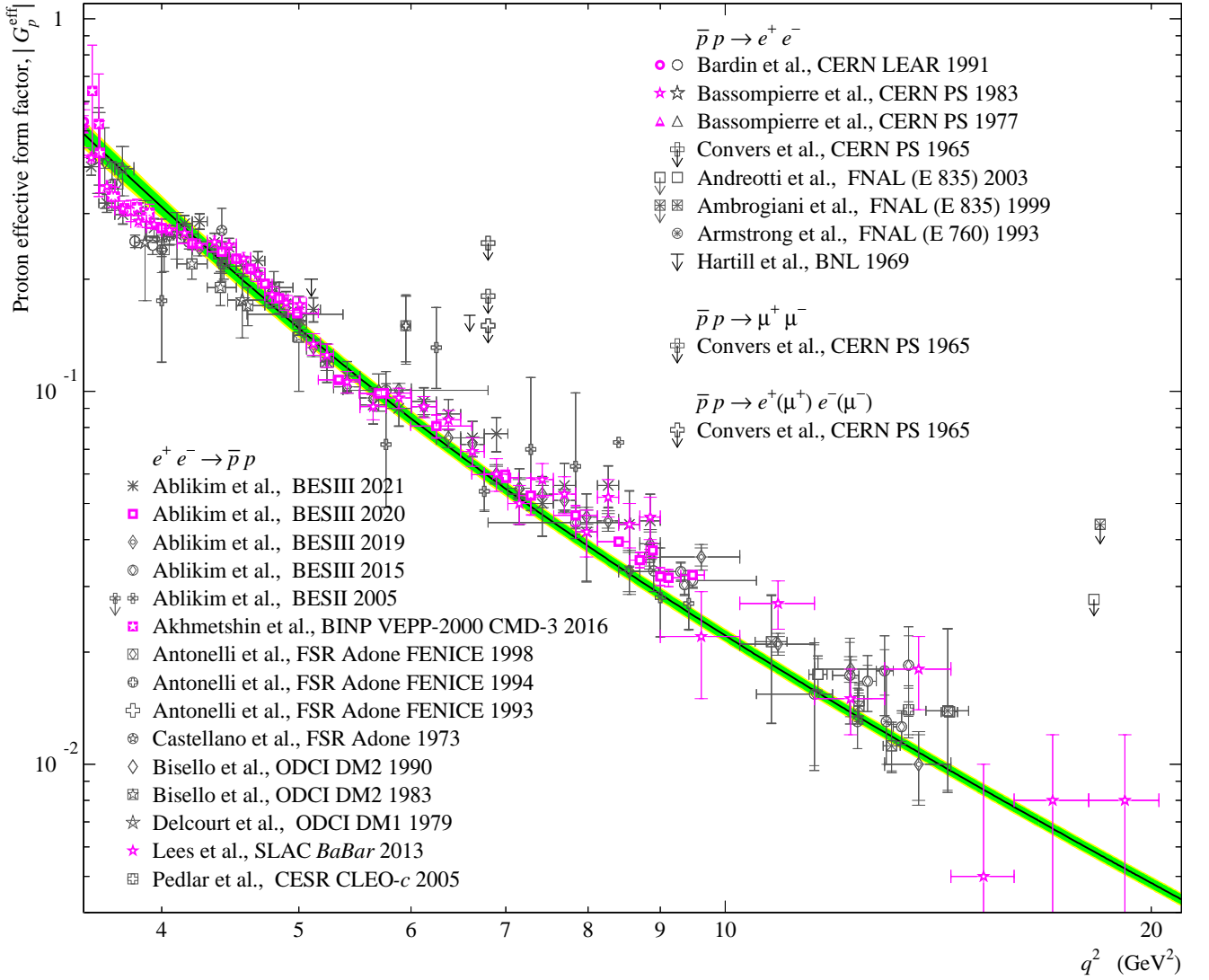


Figure 5. Proton effective form factor (3.1) measured for the timelike region with BESIII 2021 [35], 2020 [121], 2019 [120], 2015 [119], BESII 2005 [118], BINP VEPP-2000 CMD-3 [114], FSR Adone FENICE 1998 [110], 1994 [29], 1993 [28], Adone 1973 [21], OSCI ISR DM2 1990 [106, 107], 1983 [26], DM1 1979 [27], SLAC *BaBar* [85], and CESR CLEO-*c* 2005 [90] from the analysis of $e^+e^- \rightarrow \bar{p}p$ reaction, CERN LEAR 1991 [112], PS 1983 [111], 1977 [23], 1965 [24], FNAL (E 835) 2003 [82], 1999 [84], (E 760) 1993 [83], and BNL 1969 [25] from the analysis of $\bar{p}p \rightarrow e^+e^-$ reaction in comparison with the eVMD-VI model. The data of BNL 1969 [25], BES 2005 [118] measured at $\sqrt{s} = 2.9 \text{ GeV}$, and the last data points of FNAL (E 835) [82, 84] are constraints for the form factor. The constraints obtained with the pioneer experiment CERN PS 1965 [24] from the analysis of $\bar{p}p \rightarrow e^+e^-$ and/or $\bar{p}p \rightarrow \mu^+\mu^-$ reactions are also shown. The data published in [27, 106, 107] are recalculated from $|G_p^2|$ data.

sideration are several points of percentage underestimated. The logarithmic singularity in the spectral function $\Im F_{1,I=1}(t)$ below the two-pion threshold contributes positively to the nucleon isovector charge radius [40, 127]. This effect is beyond the scope of the eVMD models, although taking it into account could reduce some of the deviations from the experimental data.

D. Numerical results for nucleon form factors

The nucleon form factors as functions of the four-momentum transfer squared are presented in Figs. 1 to 9. The experimental data points included in the fit are represented by shaded or partially shaded symbols, while the omitted data or data from the historical background are represented by open dark symbols. The horizontal error bars represent the experimental errors for the mean $Q^2 = -q^2$ values. The inner and outer vertical error bars indicate statistical and total errors, respectively. The colored uncertainty bands surrounding the curves represent

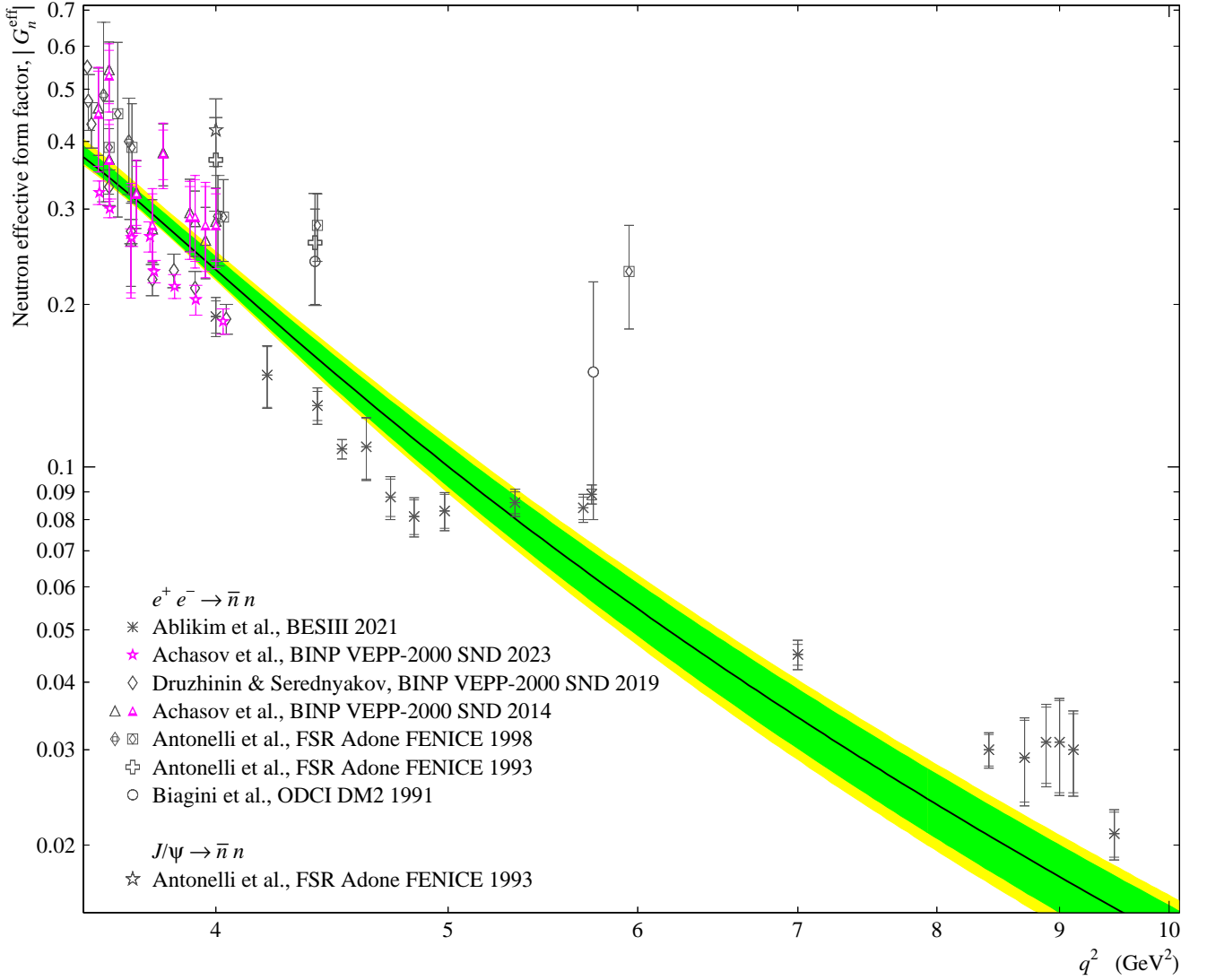


Figure 6. Neutron effective form factor (3.1) measured for the timelike region with BESIII 2021 [122], BINP VEPP-2000 SND 2023 [36, 116], 2019 [115], 2014 [113], FSR Adone FENICE 1998 [110] (data point measured at $q^2 = 3.61 \text{ GeV}^2$ as the 68% C.L. limit of the form factor is borrowed from [113] and shown here for completeness), 1993 [28], and OSCI ISR DM2 [108] from the analysis of $e^+ e^- \rightarrow \bar{n} n$ reaction, FENICE 1993 [109] from the analysis of $J/\psi \rightarrow \bar{n} n$ reaction in comparison with the eVMD-VI model. Data published in [115] and [113] (marked as open triangle) are borrowed from [122].

the 1σ and 2σ confidence intervals of the form factors determined by the correlated statistical errors of the fitted parameters of the eVMD-VI model. Different form factors and ratios have different uncertainty band widths. The reason for this is that the fitted parameter contours for the correlated errors of the electric and magnetic proton and neutron form factors are not symmetrical and exhibit different ellipsoid features.

Figure 1 shows modules of the electric and magnetic form factors of the proton and neutron predicted within the eVMD-VI model for positive and negative values of $t = q^2$ in comparison with the world experimental data. The peaks generated by vector mesons determine the nontrivial behavior of the form factors in the region $0 < t < 4m_N^2$. The magnitudes and layout of the

peaks are regulated by the masses and widths of the mesons. The eVMD-VI model predicts a smooth decline of the form factors at large positive values of Q^2 to which the cross sections of lepton–nucleon interactions are sensitive. The non-physical region $0 < t < 4m_N^2$ is inaccessible for direct measurement of form factors. In this region, meson resonances generate narrow peaks that are represented by the Breit-Wigner formula with an energy-dependent width. Residues control the phases of the resonance contributions at the poles, which in turn influence the interference of vector mesons.

Figures 2 to 9 show the eVMD-VI model predictions for the proton and neutron form factors in comparison with the experimental data on an enlarged scale to illustrate the absolute values and asymptotic behavior.

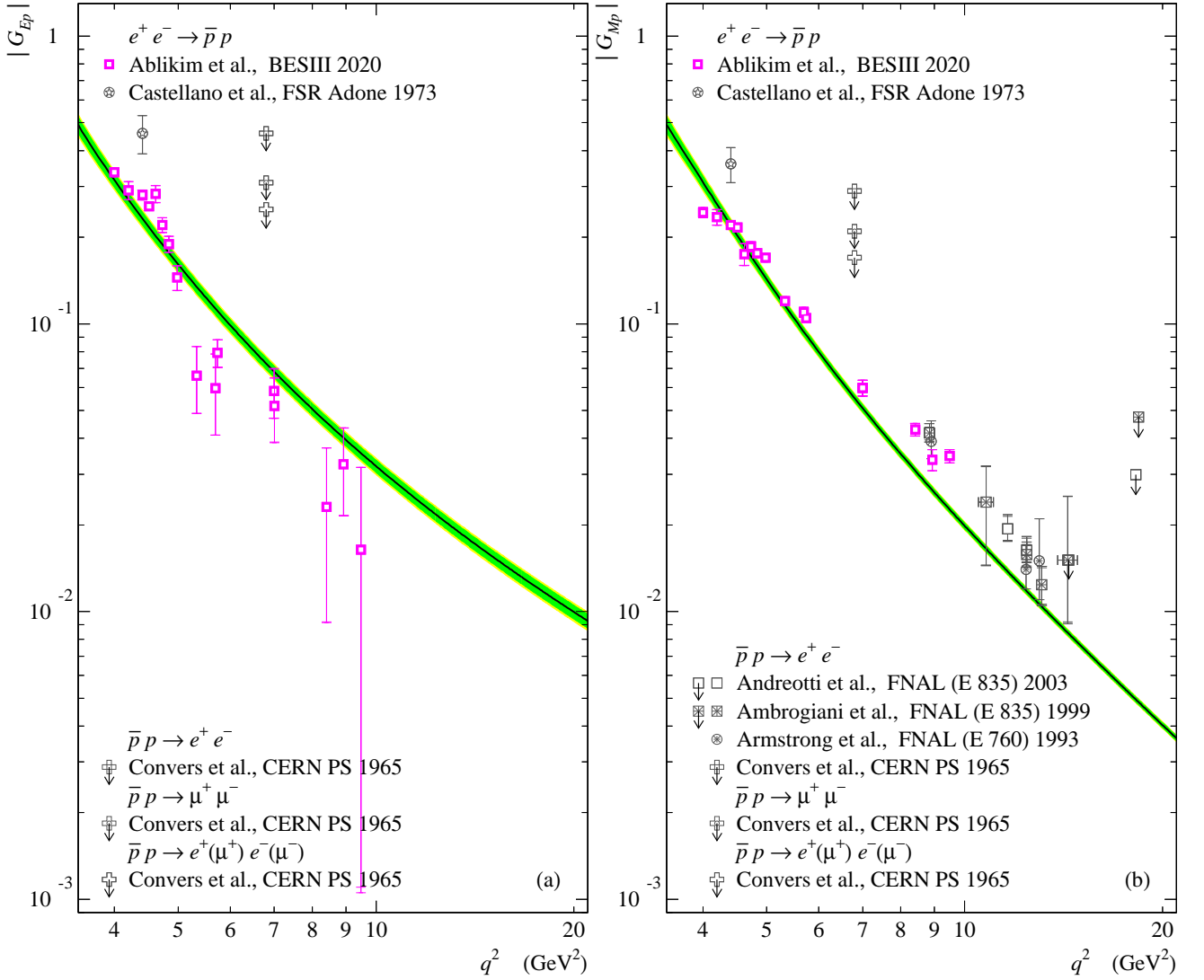


Figure 7. Modules of electric (a) and magnetic (b) form factors of the proton measured for the timelike region with BESIII 2020 [121] and FSR Adone 1973 [21] from the analysis of $e^+e^- \rightarrow \bar{p}p$ reaction, FNAL (E 835) 2003 [82], 1999 [84], and (E 760) 1993 [83] from the analysis of $\bar{p}p \rightarrow e^+e^-$ reaction in comparison with the eVMD-VI model. The limits obtained with CERN PS 1965 [24] from the analysis of $\bar{p}p \rightarrow e^+e^-$ or/and $\bar{p}p \rightarrow \mu^+\mu^-$ reactions also shown.

The electric form factor of the proton normalized by the standard dipole function (1.4) is shown in Fig. 2 in comparison with the experimental data measured for record low values of Q^2 . The experimental data and model predictions are well consistent with the dipole dependence of the form factors on Q^2 in this region. Additional data on measuring this ratio at high Q^2 values could allow to reliably fine-tune parameters of the eVMD models.

In the space-like region, the eVMD-VI model qualitatively reproduces the Q^2 dependence of the proton magnetic form factor, as shown in Fig. 3(a), for $Q^2 \lesssim 10$ GeV². The model curve has a local maximum at 1 GeV², while the experimental data corresponds to a maximum at around 2 GeV², with the latter being more pronounced. The deviations from the model curve are not

more than 5%. Fig. 4(b) shows a similar structure in the neutron magnetic form factor, which could be associated with a more sophisticated version of the spectral function of nucleon form factors. The ratio of the proton electric and magnetic form factors shown in Fig. 3(b) is reproduced reasonably well for $Q^2 \lesssim 2$ GeV², but differs from that implied by the JLab data at higher momentum transfers. The deviation is partly due to the relatively large experimental errors and the resulting lower statistical weighting compared to other data included in the fit. New accurate measurements of the ratio at high values of Q^2 are essential to refine the analysis. Fig. 3(b) shows that the range of applicability of the SR's is limited by the values of $Q^2 \lesssim 2$ GeV².

As demonstrated in Fig. 4(c), the eVMD-VI model yields the neutron electric form factor consistent with the

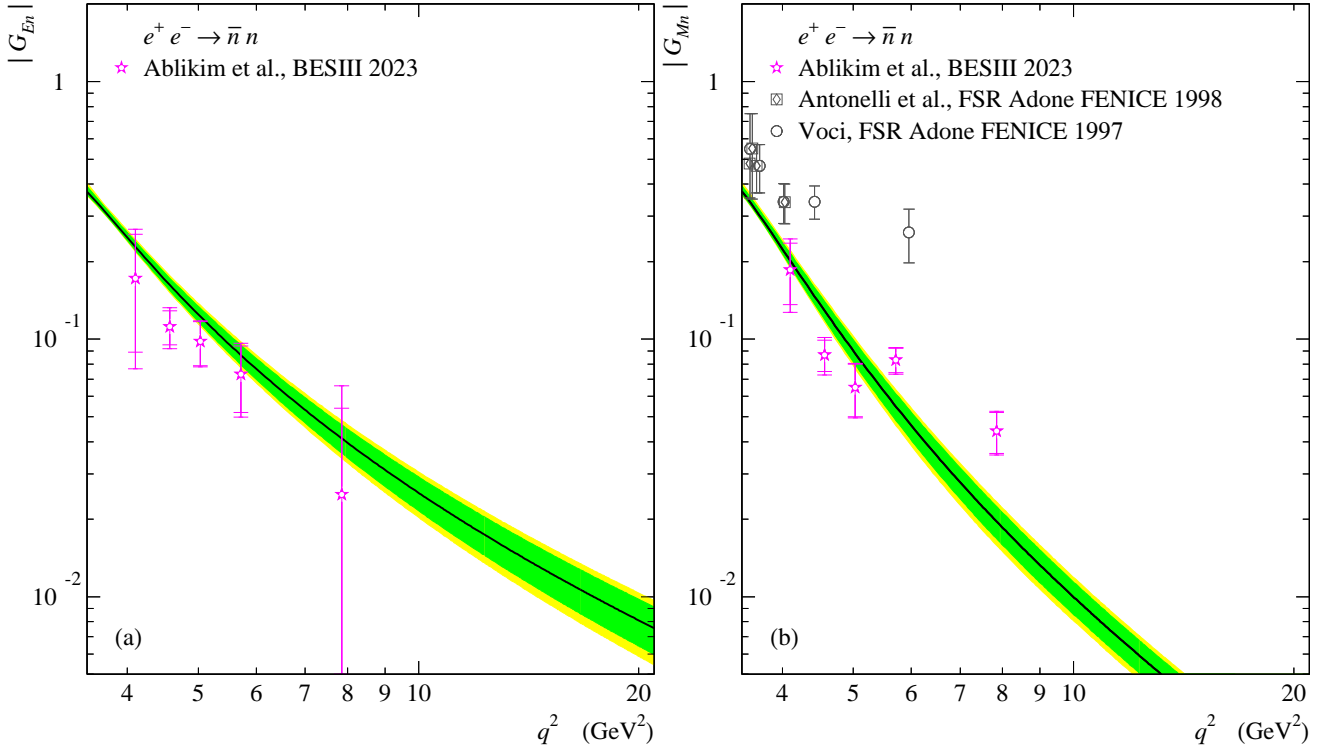


Figure 8. Modules of electric (a) and magnetic (b) form factor of the neutron measured for the timelike region with BESIII 2023 [123], Frascati SR Adone FENICE 1998 [110] (preliminary data of 1997 [22] are shown for completeness) from the analysis of $e^+e^- \rightarrow \bar{n}n$ reaction in comparison with the eVMD-VI model.

JLab data but not with the MAMI data for the spacelike region. The figure depicts the experimental findings on the neutron magnetic form factor. In the spacelike region of small Q^2 values, the eVMD-VI model agrees with the data obtained from the SLAC experiment and predicts a smoother dependence of G_{Mn} than the MAMI experimental data. Panels (b) and (d) of the figure show that the eVMD-VI model accurately describes the ratio of the neutron electric and magnetic form factors.

The magnetic and electric form factors coincide only at $t = 4m_N^2$, so the results of experiments, obtained assuming $|G_{ET}(t)| = |G_{MT}(t)|$ in the time-like region, are not included in the statistical analysis.

Recent experimental data from BESIII and BIND on the effective nucleon form factors indicate the presence of sinusoidal modulations in their behavior. In the case of a proton, sinusoidal modulations can be seen quite clearly in Fig. 5. Bianconi and Tomasi-Gustafsson [137] discovered their existence by analyzing data from the *BaBar* Collaboration [85, 138]. The effective neutron form factor data shown in Fig. 6 has significantly higher experimental errors compared to the effective proton form factor data. The presence of an irregular structure at $q^2 \sim 5 \text{ GeV}^2$ is clearly visible. The sinusoidal modulations observed by the BESIII Collaboration in the effective neutron form factor do not contradict the data from the SND Collaboration [36, 37]. The magnitude of the fluctuations is 10% of the regular background dependence. The physi-

cal origin of the non-monotonic behavior of the proton and neutron form factors is not entirely clear.

Bianconi and Tomasi-Gustafsson interpret the sinusoidal modulations as the result of a strong $N\bar{N}$ interaction at distances $0.7 - 1.5 \text{ fm}$. The scattering of the pair is dominated by inelastic channels, which results in a large imaginary part in the amplitude and a cross section that is close to the unitary limit [139]. The oscillations in form factors can be caused by interference of the amplitudes associated with different mechanisms, e.g., the meson and photon exchange within a $N\bar{N}$ pair on the one hand and the annihilation of a $N\bar{N}$ pair on the other.

The $N\bar{N}$ potentials are evaluated in Ref. [140] using chiral perturbation theory for both the elastic and annihilation channels.

The multiple formation of π mesons is responsible for the annihilation component of the $N\bar{N}$ scattering amplitude. The ground state and the excited states of the ρ - and ω -mesons contribute to saturating the annihilation channels. In Refs. [16, 141], the eVMD models include vector mesons with masses greater than 2 GeV . The periodic modulation of the nucleon form factors is confirmed in Ref. [16], but not in Ref. [141]. The masses and widths of vector mesons above the $N\bar{N}$ threshold, as well as their contributions to the nucleon form factors, cannot yet be determined unambiguously. Quark models provide a valuable insight into the spectrum and decay widths of excited unflavored mesons [142], which

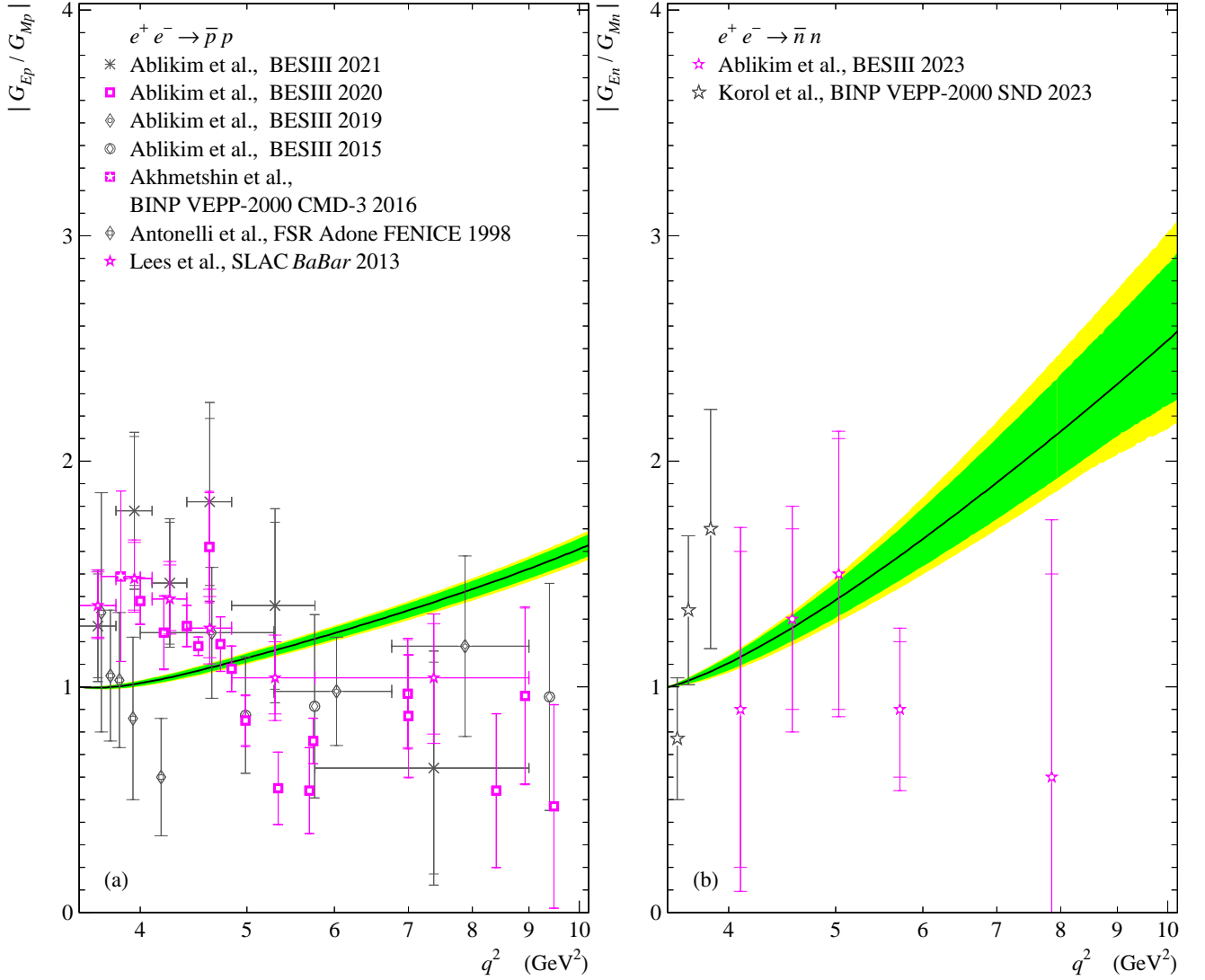


Figure 9. Modules of the ratios of electric to magnetic form factors of the proton (a) and neutron (b) measured for the timelike region with BESIII 2021 [35], 2020 [121], 2019 [120], 2015 [119], BINP VEPP-2000 CMD-3 2016 [114], Frascati SR FENICE 1998 [16, 110], SLAC *BaBar* 2013 [85] from the analysis of $e^+e^- \rightarrow \bar{p}p$ reaction and BESIII 2023 [123], BINP VEPP-2000 SND 2023 [117] from the analysis of $e^+e^- \rightarrow \bar{n}n$ reaction, respectively, in comparison with the eVMD-VI model.

can be useful for their experimental search. The eVMD-VI model describes the regular background dependence of the nucleon form factors in the time-like region. The non-monotonic structures (or so-called oscillating features) in the line shape of nucleon effective form factors cannot be reproduced without accounting for excited vector meson contributions, particularly for those with masses above the nucleon-anti-nucleon threshold.

Figures 7 and 8 show a dozen data points for the modules of electric and magnetic form factors of the nucleons in the timelike region. The errors of the proton magnetic form factor data measured in the BESIII experiment are significantly lower than the errors of the electric form factor data. The data are not qualitatively at odds with the eVMD-VI model. The model agrees better with the data obtained at the near-threshold values and generally

agrees with the data measured for high q^2 -values within the experimental errors and uncertainties of the model.

Figure 9 shows differences between model predictions and observations. Experimental results show that the ratio of electric and magnetic form factors is independent of q^2 throughout a broad range, which is one of the consequences of SR's. SR's are not followed accurately in the model under consideration. As a result, the eVMD-VI model does not follow the experimental trend well.

The presented statistical analysis uses 60 experimental data sets obtained for the form factors and their ratios. The values of χ^2/np calculated within the framework of the eVMD-VI model, where np is the number of data points in every data set, do not exceed ~ 1 for 12 experimental data sets measured with the completed MIT BLAC, MELA, CERN PS/LEAR and recent JLab ex-

periments. This group of the data includes 44 ($\sim 10\%$ of the full set) data points for G_{Ep}/G_D (18 data points), $G_{Mp}/(\mu_p G_D)$ (6), $\mu_p G_{Ep}/G_{Mp}$ (11), G_{En} (6), and $|G_p^{\text{eff}}|$ (3). The values of χ^2/np for every of 16 data sets with 62 data points ($\sim 16\%$) for $\mu_p G_{Ep}/G_{Mp}$ (22 data points), G_{En} (9), $G_{Mn}/(\mu_n G_D)$ (4), $\mu_n G_{En}/G_{Mn}$ (5), $|G_{Ep}/G_{Mp}|$ (1), $|G_{En}|$ (5), $|G_n^{\text{eff}}|$ (11), and $|G_{En}/G_{Mn}|$ (5) measured with BLAST, SLAC, JLab, MAMI, BINP, and BES experiments are less than ~ 2 . The group of 20 data sets with 186 data points (47%) for G_{Ep}/G_D (22 data points), $G_{Mp}/(\mu_p G_D)$ (37), $\mu_p G_{Ep}/G_{Mp}$ (18), G_{En} (7), $G_{Mn}/(\mu_n G_D)$ (10), $\mu_n G_{En}/G_{Mn}$ (3), $|G_{Ep}|$ (16), $|G_p^{\text{eff}}|$ (48), $|G_{Ep}/G_{Mp}|$ (22), and $|G_{Mn}|$ (5) measured with BLAST, SLAC, JLab, NIKHEF, MAMI, DESY, BINP, and BES experiments take values of χ^2/np exceed 10. For 12 experimental data sets with 101 data points (27%) the values of χ^2/np are higher than 10. This group of data sets mostly includes the proton form factor measured in the spacelike region.

IV. CONCLUSION

The MFK model for electromagnetic nucleon form factors has only two fitting parameters. This aspect sets it apart from parameterizations and other phenomenological models, which typically have more than a dozen fitting parameters. The need to update the earlier MFK model is brought to light by the appearance in the last decade of new data from experiments on nucleon form factors. This paper offers an upgraded version of the MFK model. The upgraded version of the model includes now an additional pair of experimentally observed non-strange vector mesons. As a result, the number of parameters to be fitted grows from two to six. This number remains still low compared to the most popular parameterizations and models. Energy-dependent decay widths of vector mesons were also taken into account. The vector meson masses and on-shell widths are equal to their experimental values, with the sole exception of the $\omega(1250)$ - and $\rho(1250)$ -mesons, the characteristics of which are not reliably determined yet.

The presented model describes well the previous data used to calculate the parameters of the MFK model and the modern data. The revised version of the model agrees well with the experimental data on proton and neutron form factors, form factor ratios, and electric and magnetic nucleon radii. The Zemach radii are also consistent with the experimental data and alternative theoretical estimations. The model's accuracy could be improved further by adding more parameters. However, as the number of parameters expands, their physical significance blurs.

In the time-like region, the eVMD-VI model accurately reproduces the regular component of the nucleon form factors. The contribution of excited vector mesons with masses above the $N\bar{N}$ threshold appears to be essential for replicating the periodic modulations in the nucleon-

form factors.

The analysis of the nucleon form factors performed in this work is also aimed at identifying physical effects that influence the form factors' behavior. Such effects are the quark counting rules, the Okubo-Zweig-Iizuka rule, and the scaling laws of Sachs form factors for low and moderate momentum transfers. The coupling constants of ρ -mesons with nucleons found in the model are consistent with the coupling constants determined within the context of dispersion theory and Frazer-Fulco unitarity. The coupling constants of ω - and ρ -mesons with nucleons also agree with phenomenological models of nucleon-nucleon interactions (Bonn model). The physical effects outlined above, as well as the model parameters associated with them, are considered to be rather well established. They can be recommended for physically justified parameterizations in numerical simulations of processes involving interactions with nucleons.

ACKNOWLEDGEMENTS

The authors thank Mrs. Galina Sandukovskaya for her help in preparing the manuscript. M. I. K. was supported by the Russian Science Foundation, project no. 23-22-00307.

APPENDIX A. DERIVATION OF EQS. (2.18) AND (2.19)

The average powers of the nucleon radii are calculated using Eqs. (2.16) and (2.17). The density distribution being averaged over the angles of \mathbf{Q} can be written in the form

$$\rho_{TN}(\mathbf{r}) = \int_0^{+\infty} \frac{4\pi Q^2 dQ}{(2\pi)^3} \frac{\sin Qr}{Qr} g_{TN}(-\mathbf{Q}^2).$$

The integrand is the even function of Q . We thus extend the integration to the interval $Q \in (-\infty, +\infty)$ and place a factor $1/2$ in front of the integral. The integral is non-singular at $Q = 0$ and it converges as $Q \rightarrow \pm\infty$, where the form factor goes to vanish. We deform the contour as shown in Fig. 10 and write $\sin Qr$ in terms of the exponents. The substitution $Q \rightarrow -Q$ in the second exponent gives, for the density distribution,

$$\int_C \frac{4\pi Q^2 dQ}{(2\pi)^3} \frac{e^{iQr}}{2iQr} g_{TN}(-\mathbf{Q}^2). \quad (\text{A.1})$$

The integrand is an analytical function in the complex Q -plane with $Q = \infty$ being the unique essential singularity. The contour C is closed in the upper half-plane, taking into account the fact that the exponential term makes the integral over the semicircle to vanish in the limit when radius of the semicircle goes to infinity.

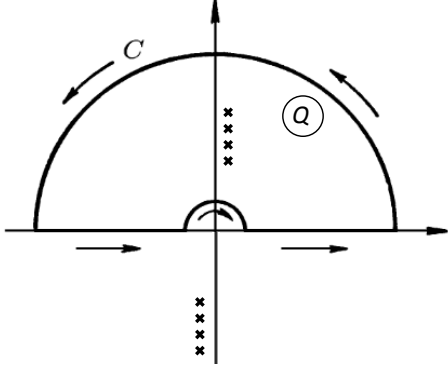


Figure 10. The directed closed curve, C , of the contour integral (A.1) in the complex Q -plane. The crosses show simple poles of the form factor $\mathcal{G}_{TN}(-\mathbf{Q}^2)$ corresponding to the vector meson masses and vector meson widths.

Now we change the order of integrals and obtain

$$\int d\mathbf{r} r^{2s+1} \frac{e^{iQr}}{2iQr} = 2\pi(-1)^{s+1} \frac{(2s+2)!}{Q^{2s+4}}, \quad (\text{A.2})$$

where $s = 0, 1, \dots$. The convergence of the integral at $r = +\infty$ is provided by the condition of $\Im(Q) > 0$.

The odd moments of the nucleon radii become

$$\langle r^{2s+1} \rangle_{TN} = (-1)^{s+1} \frac{(2s+2)!}{\pi} \int_C \frac{dQ}{Q^{2s+2}} \mathcal{G}_{TN}(-\mathbf{Q}^2).$$

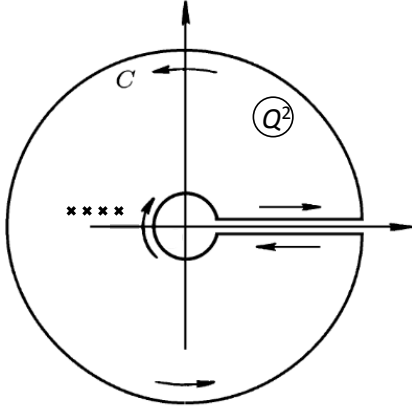


Figure 11. The contour for integration over the complex variable Q^2 . The crosses show simple poles of the form factor $\mathcal{G}_{TN}(-\mathbf{Q}^2)$.

The contour integral with a degree- s polynomial $\mathcal{P}_s(-\mathbf{Q}^2)$ substituted in place of $\mathcal{G}_{TN}(-\mathbf{Q}^2)$, vanishes identically, because there are no singularities inside of the contour C . The maximum admissible degree of $\mathcal{P}_s(-\mathbf{Q}^2)$ is determined by the condition of vanishing the integral over the infinitely distant semicircle.

Subtracting the polynomial from the form factor, $\mathcal{G}_{TN}(-\mathbf{Q}^2) \rightarrow \mathcal{G}_{TN}(-\mathbf{Q}^2) - \mathcal{P}_s(-\mathbf{Q}^2)$, does not change

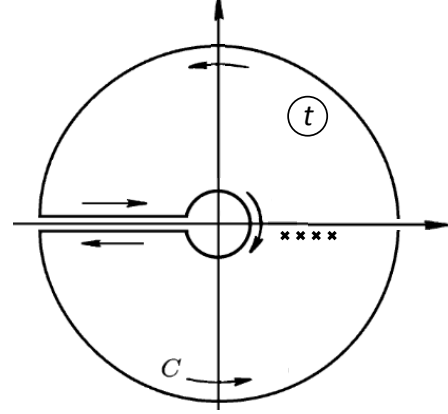


Figure 12. The contour of integration over the complex variable $t = -Q^2$. The crosses show simple poles of the form factor $\mathcal{G}_{TN}(t)$ at $t = m_V^2 - im_V \Gamma_V$.

the integral. Next, we require the integrand to be non-singular at $t = 0$. The polynomial is thereby a Taylor series of $\mathcal{G}_{TN}(-\mathbf{Q}^2)$ terminated at the highest permissible polynomial degree.

By passing to the variable Q^2 , the contour along which we integrate is altered, as illustrated in Fig. 11. Figure 12 depicts the same contour in the complex plane of $t = -Q^2$.

Equation (2.18) represents the contour integral in the form of a definite integral of a real variable.

Let us consider even powers of the nucleon radii. For a spherically symmetric density distribution, $\rho_{TN}(r)$, one has

$$\mathcal{G}_{TN}(t) = \int d\mathbf{r} \frac{\sin Qr}{Qr} \rho_{TN}(r) = \sum_{s=0}^{\infty} \frac{t^s}{(2s+1)!} \langle r^{2s} \rangle_{TN},$$

in agreement with Eq. (2.19).

The same arguments apply to the derivation of Eqs. (2.25) and (2.26).

-
- [1] W. R. Frazer and J. R. Fulco, Effect of a pion-pion scattering resonance on nucleon structure, *Phys. Rev. Lett.* **2**, 365 (1959).
 - [2] W. R. Frazer and J. R. Fulco, Effect of a pion-pion scat-

- tering resonance on nucleon structure. II, *Phys. Rev.* **117**, 1609 (1960).
- [3] W. R. Frazer and J. R. Fulco, Partial-wave dispersion relations for the process $\pi + \pi \rightarrow N + \bar{N}$, *Phys. Rev.* **117**,

- 1603 (1960).
- [4] G. Gounaris and J. J. Sakurai, Finite-width corrections to the vector-meson-dominance prediction for $\rho \rightarrow e^+e^-$, *Phys. Rev. Lett.* **21**, 244 (1968).
 - [5] V. A. Matveev, R. M. Muradyan, and A. V. Tavkhelidze, Automodelism in the large-angle elastic scattering and structure of hadrons, *Lett. Nuovo Cim.* **7**, 719 (1973).
 - [6] S. J. Brodsky and G. R. Farrar, Scaling laws at large transverse momentum, *Phys. Rev. Lett.* **31**, 1153 (1973).
 - [7] S. J. Brodsky and G. R. Farrar, Scaling laws for large-momentum-transfer processes, *Phys. Rev. D* **11**, 1309 (1975).
 - [8] A. I. Vainshtein and V. I. Zakharov, Remarks on the electromagnetic form factors of hadrons in the quark model, *Phys. Lett. B* **72**, 368 (1978).
 - [9] E. Santini, M. D. Cozma, A. Faessler, C. Fuchs, M. I. Krivoruchenko, and B. Martemyanov, Dilepton production in heavy-ion collisions with in-medium spectral functions of vector mesons, *Phys. Rev. C* **78**, 034910 (2008).
 - [10] R. P. Feynman, *Photon-hadron interactions* (W. A. Benjamin, Inc., Reading, Massachusetts, USA, 1972).
 - [11] J. G. Körner and M. Kuroda, e^+e^- annihilation into baryon-antibaryon pairs, *Phys. Rev. D* **16**, 2165 (1977).
 - [12] A. Faessler, C. Fuchs, and M. I. Krivoruchenko, Dilepton spectra from decays of light unflavored mesons, *Phys. Rev. C* **61**, 035206 (2000), arXiv:nucl-th/9904024.
 - [13] A. Faessler, C. Fuchs, M. I. Krivoruchenko, and B. V. Martemyanov, Dilepton production in proton-proton collisions at BEVALAC energies, *J. Phys. G* **29**, 603 (2003), arXiv:nucl-th/0010056.
 - [14] B. V. Martemyanov, A. Faessler, and M. I. Krivoruchenko, Electromagnetic form factors of nucleons in the extended vector meson dominance model, *Phys. Rev. C* **82**, 038201 (2010), 0910.5589 [hep-ph].
 - [15] M. I. Krivoruchenko, B. V. Martemyanov, A. Faessler, and C. Fuchs, Electromagnetic transition form factors and dilepton decay rates of nucleon resonances, *Annals Phys.* **296**, 299 (2002), arXiv:nucl-th/0110066.
 - [16] Y.-H. Lin, H.-W. Hammer, and U.-G. Meißner, New insights into the nucleon's electromagnetic structure, *Phys. Rev. Lett.* **128**, 052002 (2022), 2109.12961 [hep-ph].
 - [17] J. J. Kelly, Simple parametrization of nucleon form factors, *Phys. Rev. C* **70**, 068202 (2004).
 - [18] S. Galster *et al.*, Elastic electron-deuteron scattering and the electric neutron form factor at four-momentum transfers $5 \text{ fm}^{-2} < q^2 < 14 \text{ fm}^{-2}$, *Nucl. Phys. B* **32**, 221 (1971).
 - [19] R. K. Jr. Bradford, A. Bodek, H. S. Budd, and J. R. Arrington, A new parameterization of the nucleon elastic form factors, *Proceedings of the 4th International Workshop on Neutrino-Nucleus Interactions in the Few GeV Region (NuInt 2005)*, Okayama, Japan, September 26–29, 2005, *Nucl. Phys. (Proc. Suppl.)* **159**, 127 (2006), arXiv:hep-ex/0602017.
 - [20] A. Bodek, S. Avvakumov, R. Bradford, and H. S. Budd, Vector and axial nucleon form factors: A duality constrained parameterization, *Eur. Phys. J. C* **53**, 349 (2008), 0708.1946 [hep-ex].
 - [21] M. Castellano *et al.*, The reaction $e^+e^- \rightarrow \bar{p}p$ at a total energy of 2.1 GeV, *Il Nuovo Cim.* **14 A**, 1 (1973).
 - [22] C. Voci (on behalf of FENICE Collaboration), The first measurement of the neutron electromagnetic form factors in the time-like region, *Nucl. Phys. A* **623**, 333c (1997).
 - [23] G. Bassompierre (Mulhouse–Strasbourg–Turin Collaboration), First determination of the proton electromagnetic form factors at the threshold of the time-like region, *Phys. Lett.* **68B**, 477 (1977).
 - [24] M. Conversi, T. Massam, A. Zichichi, and T. Muller, The leptonic annihilation modes of the proton-antiproton system, at $6.8 (\text{GeV}/c)^2$ timelike four-momentum transfer, *Il Nuovo Cim.* **XL A**, 690 (1965).
 - [25] D. L. Hartill *et al.*, Antiproton-proton annihilation into electron-positron pairs and gamma-ray pairs, *Phys. Rev.* **184**, 1415 (1969).
 - [26] D. Bisello *et al.*, A measurement of $e^+e^- \rightarrow \bar{p}p$ for $(1975 \leq \sqrt{s} \leq 2250) \text{ MeV}$, *Nucl. Phys. B* **224**, 379 (1983).
 - [27] B. Delcourt *et al.*, Study of the reaction $e^+e^- \rightarrow p\bar{p}$ in the total energy range 1925 – 2180 MeV, *Phys. Lett.* **86 B**, 395 (1979).
 - [28] A. Antonelli *et al.*, First measurement of the neutron electromagnetic form factor in the time-like region, *Phys. Lett. B* **313**, 283 (1993).
 - [29] A. Antonelli *et al.*, Measurement of the electromagnetic form factor of the proton in the time-like region, *Phys. Lett. B* **334**, 431 (1994).
 - [30] V. Punjabi *et al.*, The structure of the nucleon: Elastic electromagnetic form factors, *Eur. Phys. J. A* **51**, 79 (2015), 1503.01452 [nucl-ex].
 - [31] A. Denig and G. Salme, Nucleon electromagnetic form factors in the timelike region, *Prog. Part. Nucl. Phys.* **68**, 113 (2013), 1210.4689 [hep-ex].
 - [32] S. Pacetti, R. Baldini Ferroli, and E. Tomasi-Gustafsson, Proton electromagnetic form factors: Basic notions, present achievements and future perspectives, *Phys. Rep.* **550–551**, 1 (2015).
 - [33] J. D. Bjorken and S. D. Drell, *Relativistic quantum mechanics* (McGraw-Hill Inc., New York City, New York, USA, 1964).
 - [34] B. V. Geshkenbein, Analysis of experiments on the measurement of the pion electromagnetic formfactor, *Z. Phys. C* **45**, 351 (1989).
 - [35] M. Ablikim *et al.* (BESIII Collaboration), Measurement of proton electromagnetic form factors in the time-like region using initial state radiation at BESIII, *Phys. Lett. B* **817**, 136328 (2021), 2102.10337 [hep-ex].
 - [36] M. N. Achasov *et al.*, Measurements of the neutron timelike electromagnetic formfactor with the SND detector, *Phys. Atom. Nucl.* **86**, 1165 (2023), 2309.05241 [hep-ex].
 - [37] M. N. Achasov *et al.* (SND Collaboration), Experimental study of the $e^+e^- \rightarrow n\bar{n}$ process at the VEPP-2000 e^+e^- Collider with the SND detector, *Eur. Phys. J. C* **82**, 761 (2022), 2206.13047 [hep-ex].
 - [38] D. J. Griffiths, *Introduction to elementary particles* (WILEY-VCH Verlag GmbH & Co. KGaA, Weinheim, Germany, 2008 (second, revised ed.)).
 - [39] D. V. Shirkov, V. V. Serebryakov, and V. A. Mescheryakov, *Dispersion theories of strong interactions at low energy* (North-Holland Publishing Co., Amsterdam, The Netherlands, 1969).

- [40] G. Höhler, *Pion–nucleon scattering* (Springer, Landolt-Börnstein, Switzerland, 1983).
- [41] Y.-H. Lin, H.-W. Hammer, and U.-G. Meißner, Dispersion-theoretical analysis of the electromagnetic form factors of the nucleon: Past, present and future, *Eur. Phys. J. A* **57**, 255 (2021), 2106.06357 [hep-ph].
- [42] P. D. B. Collins, *An introduction to Regge theory and high energy physics* (Cambridge University Press, Cambridge, England, 2023).
- [43] J. J. Sakurai and D. Schildknecht, Generalized vector dominance and inelastic electron–proton scattering, *Phys. Lett.* **40B**, 121 (1972).
- [44] G. Höhler *et al.*, Analysis of electromagnetic nucleon form factors, *Nucl. Phys. B* **114**, 505 (1976).
- [45] M. A. Belushkin, H.-W. Hammer, and U.-G. Meißner, Dispersion analysis of the nucleon form factors including meson continua, *Phys. Rev. C* **75**, 035202 (2007), arXiv:hep-ph/0608337.
- [46] B. Yan, C. Chen, and J.-J. Xie, Σ and Ξ electromagnetic form factors in the extended vector meson dominance model, *Phys. Rev. D* **107**, 076008 (2023), 2301.00976 [hep-ph].
- [47] Z. Ye, J. R. Arrington, R. J. Hill, and G. Lee, Proton and neutron electromagnetic form factors and uncertainties, *Phys. Lett. B* **777**, 8 (2018), 1707.09063 [nucl-ex].
- [48] C. Fuchs, M. I. Krivoruchenko, H. L. Yadav, A. Faessler, B. V. Martemyanov, and K. Shekhter, Off-shell ω production in proton–proton collisions near threshold, *Phys. Rev. C* **67**, 025202 (2003), arXiv:nucl-th/0208022.
- [49] M. Gell-Mann, D. Sharp, and W. G. Wagner, Decay rates of neutral mesons, *Phys. Rev. Lett.* **8**, 261 (1962).
- [50] S. Navas *et al.* (Particle Data Group), Review of particle physics, *Phys. Rev. D* **110**, 030001 (2024).
- [51] P. Frenkiel *et al.*, $\omega\pi$ resonances and $\pi\pi$ s-wave structures as observed in $\bar{p}p$ annihilations at rest, *Nucl. Phys. B* **47**, 61 (1972).
- [52] S. Bartalucci *et al.*, Experimental confirmation of the 1100 structure and first observation of the leptonic decay of the $\rho'(1250)$, *Nuovo Cim.* **49 A**, 207 (1979).
- [53] D. P. Barber *et al.*, Photoproduction of $\rho'(1.2)$ and $\rho'(1.6)$ in the final states $\pi^+\pi^-\pi^+\pi^-$ and $\pi^+\pi^-\pi^0\pi^0$, *Z. Phys. C* **4**, 169 (1980).
- [54] N. Hammoud, R. Kamiński, V. Nazari, and G. Rupp, Strong evidence of the $\rho(1250)$ from a unitary multichannel reanalysis of elastic scattering data with crossing-symmetry constraints, *Phys. Rev. D* **102**, 054029 (2020), 2009.06317 [hep-ph].
- [55] M. E. Christy *et al.* (Jefferson Lab E94-110 Collaboration), Measurements of electron–proton elastic cross sections for $0.4 < Q^2 < 5.5$ (GeV/c)², *Phys. Rev. C* **70**, 015206 (2004), arXiv:nucl-ex/0401030.
- [56] I. A. Qattan *et al.*, Precision Rosenbluth measurement of the proton elastic form factors, *Phys. Rev. Lett.* **94**, 142301 (2005), arXiv:nucl-ex/0410010.
- [57] G. Warren *et al.* (Jefferson Lab E93-026 Collaboration), Measurement of the electric form factor of the neutron at $Q^2 = 0.5$ and 1.0 GeV²/c², *Phys. Rev. Lett.* **92**, 042301 (2004), arXiv:nucl-ex/0308021.
- [58] V. Punjabi *et al.*, Proton elastic form factor ratios to $Q^2 = 3.5$ GeV² by polarization transfer, *Phys. Rev. C* **71**, 055202 (2005), Erratum: *ibid.* **71**, 069902 (2005), arXiv:nucl-ex/0501018.
- [59] B. Hu *et al.*, Polarization transfer in the $^2\text{H}(\vec{e}, e'\vec{p})n$ reaction up to $Q^2 = 1.61$ (GeV/c)², *Phys. Rev. C* **73**, 064004 (2006), arXiv:nucl-ex/0601025.
- [60] M. K. Jones *et al.* (Resonance Spin Structure Collaboration), Proton G_E/G_M from beam-target asymmetry, *Phys. Rev. C* **74**, 035201 (2006), arXiv:nucl-ex/0606015.
- [61] R. Madey *et al.* (Jefferson Laboratory E93-038 Collaboration), Measurements of G_E^n/G_M^n from the $^2\text{H}(\vec{e}, e'\vec{n})$ reaction to $Q^2 = 1.45$ (GeV/c)², *Phys. Rev. Lett.* **91**, 122002 (2003), arXiv:nucl-ex/0308007.
- [62] B. Plaster *et al.* (Jefferson Laboratory E93-038 Collaboration), Measurements of the neutron electric to magnetic form factor ratio G_{En}/G_{Mn} via the $^2\text{H}(\vec{e}, e', \vec{n})^1\text{H}$ reaction to $Q^2 = 1.45$ (GeV/c)², *Phys. Rev. C* **73**, 025205 (2006), arXiv:nucl-ex/0511025.
- [63] B. Anderson *et al.* (Jefferson Lab E95-001 Collaboration), Extraction of the neutron magnetic form factor from quasielastic $^3\text{He}(\vec{e}, e')$ at $Q^2 = 0.1 - 0.6$ (GeV/c)², *Phys. Rev. C* **75**, 034003 (2007), arXiv:nucl-ex/0605006.
- [64] G. MacLachlan *et al.*, The ratio of proton electromagnetic form factors via recoil polarimetry at $Q^2 = 1.13$ (GeV/c)², *Nucl. Phys. A* **764**, 261 (2006).
- [65] S. Riordan *et al.*, Measurements of the electric form factor of the neutron up to $Q^2 = 3.4$ GeV² using the reaction $^3\text{He}(\vec{e}, e'n)pp$, *Phys. Rev. Lett.* **105**, 262302 (2010), 1008.1738 [nucl-ex].
- [66] M. Meiziane *et al.* (GEP2 γ Collaboration), Search for effects beyond the Born approximation in polarization transfer observables in $\vec{e}p$ elastic scattering, *Phys. Rev. Lett.* **106**, 132501 (2011), 1012.0339 [nucl-ex].
- [67] A. J. R. Puckett *et al.*, Recoil polarization measurements of the proton electromagnetic form factor ratio to $Q^2 = 8.5$ GeV², *Phys. Rev. Lett.* **104**, 242301 (2010), arXiv:1005.3419 [nucl-ex].
- [68] M. Paolone *et al.* (E03-104 Collaboration), Polarization transfer in the $^4\text{He}(\vec{e}, e'\vec{p})^3\text{H}$ reaction at $Q^2 = 0.8$ and 1.3 (GeV/c)², *Phys. Rev. Lett.* **105**, 072001 (2010), 1002.2188 [nucl-ex].
- [69] X. Zhan *et al.*, High precision measurement of the proton elastic form factor ratio $\mu_p G_E/G_M$ at low Q^2 , *Phys. Lett. B* **705**, 59 (2011), 1102.0318 [nucl-ex].
- [70] G. Ron *et al.* (Jefferson Lab Hall A Collaboration), Low- Q^2 measurements of the proton form factor ratio $\mu_p G_E/G_M$, *Phys. Rev. C* **84**, 055204 (2011), 1103.5784 [nucl-ex].
- [71] A. J. R. Puckett *et al.*, Polarization transfer observables in elastic electron–proton scattering at $Q^2 = 2.5, 5.2, 6.8$ and 8.5 GeV², *Phys. Rev. C* **96**, 055203 (2017), Erratum: *ibid.* **98**, 019907 (2018), 1707.08587 [nucl-ex].
- [72] V. Sulkosky *et al.* (Jefferson Lab Hall A Collaboration), Extraction of the neutron electric form factor from measurements of inclusive double spin asymmetries, *Phys. Rev. C* **96**, 065206 (2017), 1704.06253 [nucl-ex].
- [73] A. Liyanage *et al.* (SANE Collaboration), Proton form factor ratio $\mu_p G_E^p/G_M^p$ from double spin asymmetry, *Phys. Rev. C* **101**, 035206 (2020), 1806.11156 [nucl-ex].
- [74] M. E. Christy *et al.*, Form factors and two-photon exchange in high-energy elastic electron–proton scattering, *Phys. Rev. Lett.* **128**, 102002 (2022), 2103.01842 [nucl-ex].
- [75] M. K. Jones *et al.* (Jefferson Lab Hall A Collaboration), G_{Ep}/G_{Mp} ratio by polarization transfer in $\vec{e}p \rightarrow e\vec{p}$, *Phys. Rev. Lett.* **84**, 1398 (2000), arXiv:nucl-ex/9910005.

- [76] T. Janssens, R. Hofstadter, E. B. Hughes, and M. R. Yearian, Proton form factors from elastic electron–proton scattering, *Phys. Rev.* **142**, 922 (1966).
- [77] J. Litt *et al.*, Measurements of the ratio of the proton form factors, G_E/G_M at high momentum transfers and the question of scaling, *Phys. Lett.* **31B**, 40 (1970).
- [78] R. C. Walker *et al.*, Measurement of the proton elastic form factors for $Q^2 = 1 - 3$ (GeV/c)², *Phys. Lett. B* **224**, 353 (1989), Erratum: *ibid.* **240**, 522 (1990).
- [79] A. F. Sill *et al.*, Measurements of elastic electron–proton scattering at large momentum transfer, *Phys. Rev. D* **48**, 29 (1993).
- [80] A. Lung *et al.*, Measurements of the electric and magnetic form factors of the neutron from $Q^2 = 1.75$ to 4.00 (GeV/c)², *Phys. Rev. Lett.* **70**, 718 (1993).
- [81] L. Andivahis *et al.*, Measurements of the electric and magnetic form factors of the proton from $Q^2 = 1.75$ to 8.83 (GeV/c)², *Phys. Rev. D* **50**, 5491 (1994).
- [82] M. Andreotti *et al.*, Measurements of the magnetic form factor of the proton for timelike momentum transfers, *Phys. Lett. B* **559**, 20 (2003).
- [83] T. A. Armstrong *et al.* (E-760 Collaboration), Proton electromagnetic form factors in the timelike region from 8.9 to 13.0 GeV², *Phys. Rev. Lett.* **70**, 1212 (1993).
- [84] M. Ambrogiani *et al.*, Measurements of the magnetic form factor of the proton in the timelike region at large momentum transfer, *Phys. Rev. D* **60**, 032002 (1999).
- [85] J. P. Lees *et al.* (BaBar Collaboration), Study of $e^+e^- \rightarrow p\bar{p}$ via initial-state radiation at BABAR, *Phys. Rev. D* **87**, 092005 (2013), 1302.0055 [hep-ex].
- [86] T. Eden *et al.*, Electric form factor of the neutron from the $^2\text{H}(\vec{e}, e'\vec{n})^1\text{H}$ reaction at $Q^2 = 0.255$ (GeV/c)², *Phys. Rev. C* **50**, R1749 (1994).
- [87] B. D. Milbrath *et al.* (Bates FPP Collaboration), Comparison of polarization observables in electron scattering from the proton and deuteron, *Phys. Rev. Lett.* **80**, 452 (1998), Erratum: *ibid.* **82**, 2221 (1999), arXiv:nucl-ex/9712006.
- [88] C. B. Crawford *et al.*, Measurement of the proton’s electric to magnetic form factor ratio from $^1\vec{\text{H}}(\vec{e}, e'p)$, *Phys. Rev. Lett.* **98**, 052301 (2007), arXiv:nucl-ex/0609007.
- [89] E. Geis *et al.* (BLAST Collaboration), Charge form factor of the neutron at low momentum transfer from the $^2\vec{\text{H}}(\vec{e}, e'n)^1\text{H}$ reaction, *Phys. Rev. Lett.* **101**, 042501 (2008), 0803.3827 [nucl-ex].
- [90] T. K. Pedlar *et al.* (CLEO Collaboration), Precision measurements of the timelike electromagnetic form factors of pion, kaon, and proton, *Phys. Rev. Lett.* **95**, 261803 (2005), arXiv:hep-ex/0510005.
- [91] H. Anklin *et al.*, Precision measurement of the neutron magnetic form factor, *Phys. Lett. B* **336**, 313 (1994).
- [92] I. Passchier *et al.*, Charge form factor of the neutron from the reaction $^2\vec{\text{H}}(\vec{e}, e'n)p$, *Phys. Rev. Lett.* **82**, 4988 (1999), arXiv:nucl-ex/9907012.
- [93] I. Passchier *et al.*, The charge form factor of the neutron from $^2\vec{\text{H}}(\vec{e}, e'n)p$, *Nucl. Phys. A* **663&664**, 421c (2000), arXiv:nucl-ex/9908002.
- [94] W. Bartel *et al.*, Measurement of proton and neutron electromagnetic form factors at squared four-momentum transfers up to 3 (GeV/c)², *Nucl. Phys. B* **58**, 429 (1973).
- [95] C. Berger *et al.*, Electromagnetic form factors of the proton at squared four-momentum transfers between 10 and 50 fm^{−2}, *Phys. Lett.* **35B**, 87 (1971).
- [96] F. Borkowski *et al.*, Electromagnetic form factors of the proton at low four-momentum transfer (II), *Nucl. Phys. B* **93**, 461 (1975).
- [97] H. Anklin *et al.*, Precise measurements of the neutron magnetic form factor, *Phys. Lett. B* **428**, 248 (1998).
- [98] C. Herberg *et al.*, Determination of the neutron electric form factor in the $D(e, e'n)p$ reaction and the influence of nuclear binding, *Eur. Phys. J. A* **5**, 131 (1999).
- [99] D. Rohe *et al.*, Measurement of the neutron electric form factor G_{en} at 0.67 (GeV/c)² via $^3\vec{\text{He}}(\vec{e}, e'n)$, *Phys. Rev. Lett.* **83**, 4257 (1999).
- [100] T. Pospischil *et al.*, Measurement of G_{Ep}/G_{Mp} via polarization transfer at $Q^2 = 0.4$ GeV/c², *Eur. Phys. J. A* **12**, 125 (2001).
- [101] G. Kubon *et al.*, Precise neutron magnetic form factors, *Phys. Lett. B* **524**, 26 (2002), arXiv:nucl-ex/0107016.
- [102] B. S. Schlimme *et al.*, Measurement of the neutron electric to magnetic form factor ratio at $Q^2 = 1.58$ GeV² using the reaction $^3\vec{\text{He}}(\vec{e}, e'n)pp$, *Phys. Rev. Lett.* **111**, 132504 (2013), 1307.7361 [nucl-ex].
- [103] M. Mihovilović *et al.*, First measurement of proton’s charge form factor at very low Q^2 with initial state radiation, *Phys. Lett. B* **771**, 194 (2017), 1612.06707 [nucl-ex].
- [104] F. Borkowski *et al.*, Electromagnetic form factors of the proton at low four-momentum transfer, *Nucl. Phys. A* **222**, 269 (1974).
- [105] G. G. Simon, C. Schmitt, F. Borkowski, and V. H. Walther, Absolute electron–proton cross sections at low momentum transfer measured with a high pressure gas target system, *Nucl. Phys. A* **333**, 381 (1980).
- [106] A. Castro *et al.*, The π , K , proton electromagnetic form factors and new related DM2 results, in *Proceedings of the Nucleon Structure Workshop: FENICE Experiment and Investigation of the Neutron Form Factor, 27–28 October 1988, Frascati, Italy, Printed and published by Servizio Documentazione dei Laboratori Nazionali di Frascati, Ed. Mrs. L. Invidia, 1988*, LAL 88-58.
- [107] D. Bisello *et al.* (DM2 Collaboration), Baryon pairs production in e^+e^- annihilation at $\sqrt{s} = 2.4$ GeV, *Z. Phys. C* **48**, 23 (1990).
- [108] M. E. Biagini, E. Pasqualucci, and A. Rotondo, U -spin considerations to guess the unknown time-like neutron form factors, *Z. Phys. C* **52**, 631 (1991).
- [109] A. Antonelli *et al.*, A new measurement of $J/\psi \rightarrow n\bar{n}$, *Phys. Lett. B* **301**, 317 (1993).
- [110] A. Antonelli *et al.*, The first measurement of the neutron electromagnetic form factors in the time-like region, *Nucl. Phys. B* **517**, 3 (1998).
- [111] G. Bassompierre *et al.*, Electron–positron pair production in $\bar{p}p$ annihilation at rest and related determination of the electromagnetic form factor of the proton in the timelike region, *Il Nuovo Cim.* **73A**, 348 (1983).
- [112] G. Bardin *et al.*, Measurement of the proton electromagnetic form factor near threshold in the time-like region, *Phys. Lett. B* **255**, 149 (1991).
- [113] M. N. Achasov *et al.*, Study of the process $e^+e^- \rightarrow n\bar{n}$ at the VEPP-2000 e^+e^- Collider with the SND detector, *Phys. Rev. D* **90**, 112007 (2014), 1410.3188 [hep-ex].
- [114] R. R. Akhmetshin *et al.*, Study of the process $e^+e^- \rightarrow p\bar{p}$ in the c.m. energy range from threshold to 2 GeV with the CMD-3 detector, *Phys. Lett. B* **759**, 634 (2016),

- 1507.08013 [hep-ex].
- [115] V. P. Druzhinin and S. I. Serednyakov, Measurement of the $e^+e^- \rightarrow n\bar{n}$ cross section with the SND detector at the VEPP-2000 Collider, *Eur. Phys. J. Web of Conf.* **212**, 07007 (2019).
 - [116] M. N. Achasov *et al.*, Experimental study of the $e^+e^- \rightarrow n\bar{n}$ process at the VEPP-2000 Collider with the SND detector, *Phys. Part. Nucl.* **54**, 624 (2023).
 - [117] A. A. Korol *et al.*, Recent SND experiment results on e^+e^- annihilation to hadrons, *Int. J. Mod. Phys.: Conf. Ser.* **51**, 2361005 (2023).
 - [118] M. Ablikim *et al.* (BES Collaboration), Measurement of the cross section for $e^+e^- \rightarrow p\bar{p}$ center-of-mass energies from 2.0 to 3.07 GeV, *Phys. Lett. B* **630**, 14 (2005), arXiv:hep-ex/0506059.
 - [119] M. Ablikim *et al.* (BESIII Collaboration), Measurement of the proton form factor by studying $e^+e^- \rightarrow p\bar{p}$, *Phys. Rev. D* **91**, 112004 (2015), 1504.02680 [hep-ex].
 - [120] M. Ablikim *et al.* (BESIII Collaboration), Study of the process $e^+e^- \rightarrow p\bar{p}$ via initial state radiation at BESIII, *Phys. Rev. D* **99**, 092002 (2019), 1902.00665 [hep-ex].
 - [121] M. Ablikim *et al.* (BESIII Collaboration), Measurement of proton electromagnetic form factors in $e^+e^- \rightarrow p\bar{p}$ in the energy region 2.00–3.08 GeV, *Phys. Rev. Lett.* **124**, 042001 (2020), 1905.09001 [hep-ex].
 - [122] M. Ablikim *et al.* (BESIII Collaboration), Oscillating features in the electromagnetic structure of the neutron, *Nature Phys.* **17**, 1200 (2021), 2103.12486 [hep-ex].
 - [123] M. Ablikim *et al.* (BESIII Collaboration), Measurements of the electric and magnetic form factors of the neutron for timelike momentum transfer, *Phys. Rev. Lett.* **130**, 151905 (2023), 2212.07071 [hep-ex].
 - [124] E. J. Brash, A. Kozlov, S. Li, and G. M. Huber, New empirical fits to the proton electromagnetic form factors, *Phys. Rev. C* **65**, 051001(R) (2002), arXiv:hep-ex/0111038.
 - [125] J. R. Arrington, How well do we know the electromagnetic form factors of the proton?, *Phys. Rev. C* **68**, 034325 (2003), arXiv:nucl-ex/0305009.
 - [126] A. I. Lendel, V. I. Lendyel, V. A. Meshcheryakov, and B. M. Ernst, Influence of $\pi\pi$ -interactions on the electromagnetic structure of the nucleon, *Yad. Fiz.* **3**, 1093 (1966).
 - [127] G. Höhler and E. Pietarinen, The ρNN vertex in vector-dominance model, *Nucl. Phys. B* **95**, 210 (1975).
 - [128] M. I. Krivoruchenko, Analytical extension of the Frazer-Fulco unitarity relations for isovector nucleon form factors to the complex t -plane, arXiv:nucl-th/9710072.
 - [129] R. Machleidt, K. Holinde, and C. Elster, The Bonn meson exchange model for the nucleon–nucleon interaction, *Phys. Rept.* **149**, 1 (1987).
 - [130] F. James, *MINUIT – function minimization and error analysis: Reference manual version 94.1* (1994), CERN-D-506.
 - [131] F. James and M. Roos, MINUIT – a system for function minimization and analysis of the parameter errors and correlations, *Comput. Phys. Commun.* **10**, 343 (1975).
 - [132] G. Cowan, *Statistical data analysis* (Clarendon Press Pub., Oxford University Press Inc., Oxford, England, 1998).
 - [133] M. O. Distler, J. C. Bernauer, and T. Walcher, The RMS charge radius of the proton and Zemach moments, *Phys. Lett. B* **696**, 343 (2011), 1011.1861 [nucl-th].
 - [134] J. C. Bernauer *et al.* (A1 Collaboration), High-precision determination of the electric and magnetic form factors of the proton, *Phys. Rev. Lett.* **105**, 242001 (2010), 24:1007.5076 [nucl-ex].
 - [135] J. Arrington, W. Melnitchouk, and J. A. Tjon, Global analysis of proton elastic form factor data with two-photon exchange corrections, *Phys. Rev. C* **76**, 035205 (2007), 0707.1861 [nucl-ex].
 - [136] J. L. Friar and I. Sick, Muonic hydrogen and the third Zemach moment, *Phys. Rev. A* **72**, 040502(R) (2005), arXiv:nucl-th/0508025.
 - [137] A. Bianconi and E. Tomasi-Gustafsson, Periodic interference structures in the timelike proton form factor, *Phys. Rev. Lett.* **114**, 232301 (2015), 1503.02140 [nucl-th].
 - [138] J. P. Lees *et al.* (BaBar Collaboration), Measurement of the $e^+e^- \rightarrow p\bar{p}$ cross section in the energy range from 3.0 to 6.5 GeV, *Phys. Rev. D* **88**, 072009 (2013), 1308.1795 [hep-ex].
 - [139] D. Zhou and R. G. E. Timmermans, Energy-dependent partial-wave analysis of all antiproton–proton scattering data below 925 MeV/c, *Phys. Rev. C* **86**, 044003 (2012), 1210.7074 [hep-ph].
 - [140] Q.-H. Yang, D. Guo, M.-Y. Li, L.-Y. Dai, J. Haidenbauer, and U.-G. Meißner, Study of the electromagnetic form factors of the nucleons in the timelike region, *JHEP* **08**, 208, 2404.12448 [nucl-th].
 - [141] B. Yan, C. Chen, X. Li, and J.-J. Xie, Understanding oscillating features of the time-like nucleon electromagnetic form factors within the extending vector meson dominance model, *Phys. Rev. D* **109**, 036033 (2024), 2312.04866 [nucl-th].
 - [142] L.-M. Wang, S.-Q. Luo, and X. Liu, Light unflavored vector meson spectroscopy around the mass range of 2.4 ~ 3 GeV and possible experimental evidence, *Phys. Rev. D* **105**, 034011 (2022), 2109.06617 [hep-ph].